Phytomedicine 140 (2025) 156534

Contents lists available at ScienceDirect

Phytomedicine

journal homepage: www.elsevier.com/locate/phymed

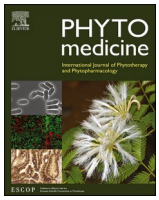

Original Article

10-Hydroxydec-2-enoic acid reduces vascular smooth muscle cell inflammation via interacting with Toll-like receptor 4

Feng Jia [a], Yongqing Wang [a], Zhiqiang Chen [a], Jingxian Jin [a], Lei Zeng [a], Li Zhang [a], Huaijian Tang [b], Yanyan Wang [b], Pei Fan [a,*]

[a] School of Biological Engineering, Henan University of Technology, Zhengzhou 450001, China
[b] School of Food and Strategic Reserves, Henan University of Technology, Zhengzhou 450001, China

ARTICLE INFO

Keywords:
10-Hydroxydec-2-enoic acid
Vascular smooth muscle cell
Toll-like receptor 4
Inflammation

ABSTRACT

Background: 10-Hydroxydec-2-enoic acid (10-HDA), a unique and marker compound in royal jelly, has a wide range of bio-activities. However, its role in regulating inflammation of vascular smooth muscle cell (VSMC), which is essential to a set of vascular diseases, is still unknown.

Purpose: Our study aimed to investigate whether 10-HDA exerts effect on VSMC inflammation via interacting with toll-like receptor 4 (TLR4), a pivotal inflammatory initiator.

Methods: A package of proteins, which might participate in TLR4-mediated signaling, influenced by 10-HDA were analyzed in mouse VSMCs with Angiotensin II(Ang II) or lipopolysaccharide (LPS) stimulation. Accordingly, pro- or anti-inflammatory cytokines, reactive oxygen species (ROS), and anti-oxidants that are closely relevant to inflammatory process were determined. The possible mode for 10-HDA interacting with TLR4 was also characterized. Moreover, involvement of a key miRNA in 10-HDA regulating VSMC inflammation was identified.

Results: In the presence of Ang II, 10-HDA inhibited the TLR4 expression in a dose-dependent manner. In such occasion, 10-HDA hindered the up-regulation of specificity protein 1 (SP1) and serine/threonine-protein phosphatase 6 catalytic subunit (PPP6C), the phosphorylation of extracellular signal-regulated kinase 1/2, TGF-β-activated kinase 1, and nuclear factor-κB p56, as well as the enhancement of myeloid differentiation primary response gene 88. Apart from SP1 and PPP6C, the level change of these proteins by 10-HDA was similar with LPS stimulation. The effect might be resulted from 10-HDA blocking TLR4 through multiple atomic interactions. 10-HDA mitigated the increase of pro-inflammatory cytokines tumor necrosis factor-alpha, interleukin-2 (IL-2), and IL-6, as well as increased the anti-inflammatory cytokine IL-10, in the Ang II- or LPS-induced VSMCs. Correspondingly, the level of ROS was attenuated and the anti-oxidants such as glutathione and superoxide dismutase were fortified. The data indicated the anti-inflammatory potential of 10-HDA in VSMCs, which was associated with 10-HDA's capability of relieving oxidative stress. Additionally, the expression of miR-17–5p was saved by 10-HDA from Ang II- or LPS-treated VSMCs, which might be relevant to SP1 and PPP6C targeting.

Conclusion: The present work of 10-HDA, for the first time, revealed its ability to alleviate VSMC inflammation by targeting TLR4 and therefore modulate the downstream inflammatory participants. Our data will cast light on the utilization of 10-HDA in VSMC inflammation-related vascular disorders.

Abbreviations: Ang II, Angiotensin II; C34, TLR4-IN-C34; DCFH-DA, 2, 7-dichlorodihydrofluorescein diacetate; DMEM, Dulbecco's Modified Eagle Medium; DMSO, dimethyl sulfoxide; ELISA, enzyme-linked immunosorbent assay; ERK1/2, extracellular signal-regulated kinase 1/2; FBS, fetal bovine serum; GSH, glutathione; IL, interleukin; LC-MS/MS, liquid chromatography-tandem mass spectrometry; LPS, lipopolysaccharide; MAPKs, mitogen-activated protein kinases; MyD88, myeloid differentiation primary response gene 88; NF-κB, nuclear factor-κB; PBS, phosphate buffered saline; PPI, protein-protein interactions; PPP6C, serine/threonine-protein phosphatase 6 catalytic subunit; P-, Phospho-; qRT-PCR, quantitative Real-Time PCR; RJ, Royal jelly; ROS, reactive oxygen species; SD, standard deviation; SDS-PAGE, sodium dodecyl sulfate-polyacrylamide gel electrophoresis; SOD, superoxide dismutase; SPs, specificity proteins; TAK1, TGF-β-activated kinase 1; TLRs, toll-like receptors; TNF-α, tumor necrosis factor-alpha; T-, Total-; VSMC, vascular smooth muscle cell; 10-HDA, 10-hydroxydec-2-enoic acid; ·OH, hydroxyl free radical.

* Corresponding author at: No. 100 Lianhua Street, Zhengzhou High-Tech Development Zone, Henan 450001, China.
E-mail address: apisfp@126.com (P. Fan).

https://doi.org/10.1016/j.phymed.2025.156534
Received 22 August 2024; Received in revised form 9 January 2025; Accepted 15 February 2025

Introduction

The pollination insect honeybee is crucial for plant ecosystem. Royal jelly (RJ) is secreted by the honeybee workers to feed the queen and the larvae within three days to ensure the continuation of the honeybee population. RJ is also a traditionally natural and functional food that consumed by human worldwide. The dry matter of RJ is mainly made up of proteins, lipids, carbohydrates, vitamins, and minerals (Collazo et al., 2021). 10-Hydroxydec-2-enoic acid (10-HDA), the unsaturated fatty acid with a hydroxyl group, is the major lipid component that exclusively exists in RJ with the ratio of 1.4–2.01%. Therefore, 10-HDA is used for evaluating RJ quality (Ma et al., 2022; Yang et al., 2017). Besides, 10-HDA is characterized by a series of bio-activities to inhibit a wide range of pathogenic bacteria and tumors. For instance, 10-HDA is capable of decreasing the biofilm viability of *Staphylococcus aureus*, and thus reducing its hemolytic effect (Gao et al., 2022). 10-HDA's anti-tumor activities are evidenced by inducing the arrest of cell cycle, as well as apoptosis, in A549 human lung cancer cells (Lin et al., 2020), and reducing the Ehrlich solid tumor in a mouse model (Albalawi et al., 2021). 10-HDA is also well-documented to protect against dysfunction in many cell types, which includes the alleviation of ultraviolet-induced damage of dermal fibroblast (Zheng et al., 2013), lipopolysaccharide (LPS)-stimulated impairment of blood-brain barrier (You et al., 2019), and cyclophosphamide-caused deterioration of thymus and spleen (Fan et al., 2020). Moreover, 10-HDA has the ability to mitigate the oxidative stress of vascular smooth muscle cell (VSMC) via scavenging hydroxyl free radical (·OH) (Fan et al., 2022), and to maintain the membrane fluidity of erythrocyte in case of ·OH toxicity (Sha et al., 2023), indicating 10-HDA's potential role in keeping health of vascular system.

Inflammation, a comprehensive process for cell's response to foreign stimuli that may be acute or chronic, is closely involved in the progression of a large variety of diseases (Arulselvan et al., 2016). VSMCs, the predominant cells integrally located in the blood vessel wall, are responsible for vascular homeostasis through contracting and relaxing movements (Leung et al., 2016; Zhu et al., 2019). The VSMC inflammation is a pivotal stage to initiate vascular disorder. The inflammatory cytokines secreted by VSMCs of proinflammatory phenotype, such as interleukin-6 (IL-6), are contributive to the infiltration of monocyte and macrophage during arteriosclerosis (Wang et al., 2022). Tumor necrosis factor-alpha (TNF-α), the other potent proinflammatory cytokine, is also up-regulated in inflammatory VSMCs (Qu and Qu, 2019; Sun and Ding, 2012). TNF-α can promote production of reactive oxygen species (ROS), and causes oxidative stress in blood vessel, thereby enhancing the risk of hypertension (Lamb et al., 2020). To find natural products that inhibit VSMC inflammation can be greatly helpful to the vascular functionality. Noticeably, the health-promoting functions of 10-HDA also include its anti-inflammatory activities in human colon cells (Yang et al., 2018), LPS-stimulated RAW 264.7 macrophage cells (Huang et al., 2022), and LPS-injected chicken *in vivo* (Han et al., 2023). However, the interconnection between 10-HDA and VSMC inflammation still remains largely unknown. Here, we aim to disclose the mode of 10-HDA in regulating inflammatory VSMCs.

Toll-like receptors (TLRs) recognize microbial pathogenic molecules and are fundamental to innate immune responses (Kawai and Akira, 2007). TLR pathway plays a central role in inflammation (Guven Maiorov et al., 2013). TLR4 had been the best understood TLR member (Rocha et al., 2016). TLR4 can be strongly activated by LPS to release critical proinflammatory cytokines (Lu et al., 2008). A subset of proteins and phospho-proteins, including the myeloid differentiation primary response gene 88 (MyD88) (Liu et al., 2020), the specificity proteins (SPs), transcription factors (MacDowell et al., 2017), as well as the phosphorylated TGF-β-activated kinase 1 (TAK1) (Wang et al., 2021), extracellular signal-regulated kinase 1/2 (ERK1/2) (J. Huang et al., 2021), and nuclear factor-κB (NF-κB) (Liu et al., 2017), engage in the TLR4 signaling pathway. Targeting TLR4 could be therapeutically beneficial to the suppression of inflammation (Coutinho-Wolino et al., 2022). In VSMCs, Angiotensin II (Ang II), a potent vasoconstrictor that causes hypertension and atherosclerosis (Jiao et al., 2023; Uchida et al., 2022), is able to up-regulate TLR4 expression and induce inflammation (Hernanz et al., 2015; S. Huang et al., 2021). Recent studies showed that 10-HDA could block TLR4 using a label-free SPR biosensor strategy, and therefore generate tolerogenic immunophenotype of dendritic cells (Eslami-Kaliji et al., 2021; Eslami-Kaliji et al., 2022). Hence, 10-HDA may act as an alleviator for VSMC inflammation via influencing the TLR4 effect. Here, our study focused on elucidating the mode of 10-HDA modulating TLR4 and its downstream molecules relevant to VSMC inflammation, which will cast light on the utilization of 10-HDA in remedying vascular dysfunctions.

Materials and methods

Cell culture

The cells used in the present study were the immortalized mouse VSMCs of C57BL/6 strain, which were purchased from American Type Culture Collection. The VSMCs were cultured in Dulbecco's Modified Eagle Medium (DMEM) (Gibco; Thermo Fisher Scientific, Inc., Waltham, MA, USA) containing 10% fetal bovine serum (FBS) (Zhejiang Tianhang Biotechnology Co., Ltd., Huzhou, Zhejiang, China) and 1% Penicillin/Streptomycin (Gibco; Thermo Fisher Scientific, Inc., Waltham, MA, USA), which was referred to as the complete media, in the environment of 37 °C and 5% CO_2. The VSMCs were subcultured using 0.25% trypsin-EDTA (Beijing Solarbio Science & Technology Co., Ltd., Beijing, China).

10-HDA treatment, and AngII or LPS challenge for VSMCs

The VSMCs cultured in the complete media grew to 80% confluent, followed by starvation for 24 h using FBS-free DMEM. Next, the VSMCs were replaced by the fresh FBS-free DMEM and treated by 10-HDA (Yuanye Bio Sci & Tech Co., Ltd., Shanghai, China) with the purity≥98% (10-HDA structure was shown in Fig. 1**A**), which was predissolved in dimethyl sulfoxide (DMSO), for 1 h. The AngII (Beijing Solarbio Science & Technology Co., Ltd., Beijing, China) or LPS (1 μg/mL) (Huang et al., 2023) (Beijing Solarbio Science & Technology Co., Ltd., Beijing, China) was then added to the cells for 6 h stimulation prior to cell collection. The same volume of DMSO without 10-HDA was added to the control VSMCs as a vehicle. In some experiments, the TLR4 inhibitor TLR4-IN-C34 (C34) (Shanghai Aladdin Biochemical Technology Co., Ltd., Shanghai, China) of 13 μM (Ji et al., 2009) was used as the positive control.

Proteomic analysis

Three groups (control, AngII, and AngII+10-HDA) of VSMCs were applied for protoemic analysis. Each group, prepared from all wells of a 6-well plate, had three replications. The final concentrations of AngII and 10-HDA were 10 μM and 4 mM, respectively. The cells were scraped down in 1 mL phosphate buffered saline (PBS), then collected by centrifugation at 1000 rpm for 3 min, and stored in -80 °C freezer.

VSMCs were ultrasonically lysed for 2 min (1 s / ultrasonication with 1 s interval) in lysis buffer (8 M carbamide, 100 mM Tris–HCl) with 2% protease inhibitor (cOmplete™ Protease inhibitor Cocktail, Roche, Basel, Switzerland). The lysates were centrifuged at 14,000 g for 20 min, the protein-containing supernatant was collected prior to the quantification of protein concentration using Bicinchoninic acid method. The quality of each protein sample (5 μg) was ensured via the analysis of sodium dodecyl sulfate-polyacrylamide gel electrophoresis (SDS-PAGE). Further, the protein of 20 μL was used to prepare peptides (including desalt) by using QLBIO MagicOmics-MMB8X kit (Beijing Qinglian Biotech Co., Ltd., Beijing, China). The prepared peptides were finally dissolved in 0.1% formic acid.

Peptides of 1 μg were analyzed through liquid chromatography-

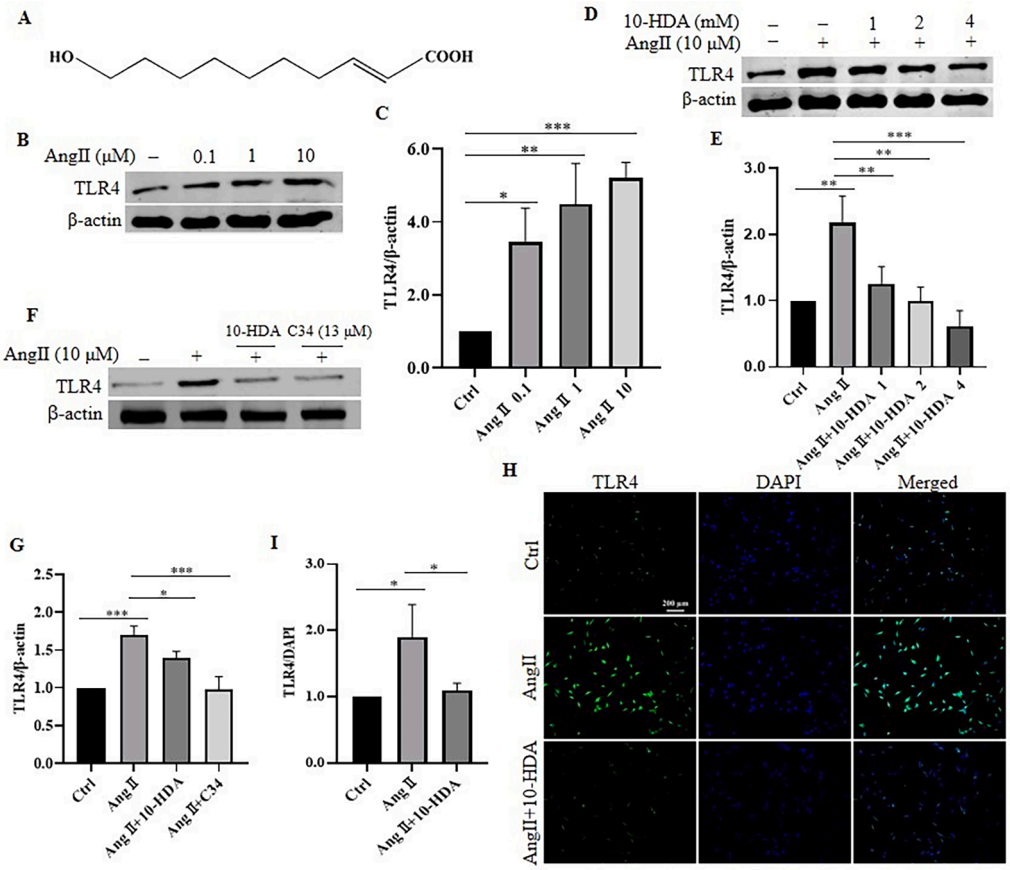

Fig. 1. 10-HDA inhibits AngII-induced TLR4 expression in VSMCs. A Chemical structure of 10-HDA. B Representative Western blots for AngII-induced TLR4 expression. The AngII doses used for treating VSMCs are 0.1 μM, 1 μM and 10 μM. C Column chart comparing the relative levels of TLR4 normalized to β-actin between VSMCs treated by different AngII doses. D Western Blots representing the TLR4 expression in AngII (10 μM)-induced VSMCs with the addition of 10-HDA at the concentrations of 1 mM, 2 mM and 4 mM. E Comparisons for the relative levels of TLR4 normalized to β-actin in AngII (10 μM)-treated VSMCs with different 10-HDA concentrations. F Western blots that represent TLR4 expression in AngII (10 μM)-induced VSMCs with the administration of 10-HDA (4 mM) or C34 (13 μM). G Relative intensity comparisons of TLR4 normalized to β-actin in VSMCs of different treatment groups. H Representative images of TLR4 and DAPI staining for VSMCs treated by AngII (10 μM) or AngII (10 μM) + 10-HDA (4 mM), in which scale bar is 200 μm. I The florescent intensity comparisons of TLR4/DAPI ratios in different VSMC groups. All data are shown as mean ± SD (n=3); *p<0.05, **p<0.01, ***p<0.001.

tandem mass spectrometry (LC-MS/MS) strategy. The mobile phase was A (0.1% formic acid) coupled with B (80% acetonitrile and 0.1% formic acid) for EASY nLC 1200 (Thermo Fisher Scientific, Inc., Waltham, MA, USA) with the self-made C_{18} column (1.5 μm, 100 μm × 250 mm) (Beijing Qinglian Biotech Co., Ltd., Beijing, China) separation, in which the ratio of B was in a gradient from 5%-12% (0 min-5 min), 12%-30% (5 min-39 min), 30%-40% (39 min-49 min), 40%-95% (49 min-50 min), and 95%-95% (50 min-60 min). The MS was the Q Exactive HF-X (Thermo Fisher Scientific, Inc., Waltham, MA, USA) with the Nanospray Flex™ ion source (electrospray ionization voltage 2.2 kV and ion transfer tube temperature 320 °C), which was in data-dependent acquisition mode using the m/z range 350–1500 and the collision energy 27. The .raw data was searched against Uniprot database of *Mus musculus* including 55,260 proteins downloaded from 2023–03–07 via Proteome Discoverer 2.4. The searching parameters were set similarly to those in the publication (Houdelet et al., 2021), except for the tolerance of 15 ppm for precursor ions, along with the fixed (Carbamidomethyl (C)) and variable (M Oxidation; Acetyl (Protein N-terminal)) modifications. A protein had the fold change >1.2 and p<0.05 between two groups was considered the differentially expressed protein. The LC-MS/MS analysis was performed in Beijing Qinglian Biotech Co., Ltd., Beijing, China. The MS .raw data were deposited in ProteomeXchange Consortium (http://proteomecentral.proteomexchange.org) (Ma et al., 2019; Chen et al., 2022b) with the dataset identifier PXD060908.

Protein-protein interactions (PPI) Network construction

The differentially expressed proteins were analyzed via the online-platform NetworkAnalyst 3.0 (https://www.networkanalyst.ca) updated on 2024–06–27 (Zhou et al., 2019). The Generic PPI Network was constructed using the built-in database of STRING Interactome. The building option was selected as First order. The Confidence score cutoff was set to 900. Subnetworks with at least 3 nodes were shown in the analysis. In addition, the Signaling Network was generated based on SIGNOR 2.0, and the Gene-miRNA Interactions was performed through Tarbase v 9.0 within the tool.

Western blotting

The VSMCs in a well of the 6-well plate were scraped down and lysed in 200 μL RIPA buffer containing 1% protease inhibitor phenylmethanesulfonyl fluoride (Beijing Solarbio Science & Technology Co., Ltd., Beijing, China) and 1% Phosphatase Inhibitor Cocktail I (100 ×) (MedChemExpress, Monmouth Junction, NJ, USA) on ice. Total protein was extracted using an ultrasonic cell homogenizer (Ningbo Scientz Biotechnology, Ningbo, Zhejiang, China). The cell lysates were centrifuged at 12,000 rpm at 4 °C for 10 min, the supernatant was sampled and quantified using the total protein assay kit (with standard: BCA method) (Nanjing Jiancheng Bioengineering Institute, Nanjing, Jiangsu, China). The protein sample was then added to 1 × loading buffer and heated at

95 °C for 5 min. A total protein of 20–40 μg was loaded for SDS-PAGE, a process using 5% stacking gel and 10% or 12% separating gel, along with 70 V for the first 25 min and 120 V for the rest. The proteins were next transferred from the gel to the PVDF membrane at 110 mA for 120 min. The membrane was blocked in 5% fat-free milk at room temperature for 1 h, and incubated with the antibody against TLR4 (Proteintech Group, Inc., Wuhan, Hubei, China), SP1 (Proteintech Group, Inc., Wuhan, Hubei, China), Serine/threonine-protein phosphatase 6 catalytic subunit (PPP6C) (ABclonal Technology Co., Ltd., Wuhan, Hubei, China), MyD88 (ABclonal Technology Co., Ltd., Wuhan, Hubei, China), Total- or Phospho-TAK1 (T- or P-TAK1), (ABclonal Technology Co., Ltd., Wuhan, Hubei, China), T- or P-ERK1/2 (Proteintech Group, Inc., Wuhan, Hubei, China), T- or P-NF-κB p56 (MedChemExpress, Monmouth Junction, NJ, USA), or β-actin (Proteintech Group, Inc., Wuhan, Hubei, China) at 4 °C overnight. Afterwards, the corresponding secondary antibody, the IRDye® 680 RD Goat anti-rabbit or anti-mouse IgG (LI-COR Biosciences, Cambridge, UK), was used at room temperature for 1 h. The blot was visualized via Odyssey® CLX system (LI-COR Biosciences, Cambridge, UK). The intensity of the band was measured through Image Studio software (Version 5.2.5, LI-COR Biotechnology, Lincoln, NE, USA).

Immuno-staining

The VSMCs were fixed in 4% paraformaldehyde in PBS for 20 min, then permeabilized by 0.2% Triton X-100 for 30 min and blocked by 5% bovine serum albumin for the other 30 min. The primary antibody against TLR4 or SP1, diluted 1: 200, was added at 4 °C overnight. The secondary antibody (1: 500) was used at room temperature for 1 h in the dark thereafter. In addition, DAPI at the dilution of 1: 1000 was applied to stain nucleus for 15 min. The cells were imaged at 10 × 20 magnification by fluorescence microscope (Axio Observer 3, Carl Zeiss, Oberkochen, Baden-Württemberg, Germany), and their fluorescent intensity was measured by image J software (Version 1.51j8, National Institutes of Health, Bethesda, MD, USA).

Molecular docking

The mouse TLR4 (UniProt No. Q8K2T5) structure was retrieved from AlphaFold Protein Structure Database (https://alphafold.ebi.ac.uk/) in the format of .pdb. Then the docking between TLR4 and 10-HDA was performed via 1-CLICK DOCKING within Mcule, the online drug discovery platform (https://mcule.com/). Serine (A:413), Lysine (A:360) and Lysine (A:263) may be the binding sites of TLR4 and LPS (Ohto et al., 2012), and their pLDDT scores (Mariani et al., 2013) in AlphaFold model were 96.12, 87.56 and 92.06, respectively. Therefore, Serine (A:413)_C3263 was selected as the binding site center (X=27.616, Y=7.564, Z=13.119) for docking with the structure of 10-HDA. The docking positions were visualized thrice using Discovery Studio 4.5 Visualizer.

Enzyme-linked immunosorbent assay (ELISA)

The VSMCs were rinsed with pre-cooled PBS and trypsinized followed by centrifugation at 1000 g for 5 min. The cell pellet was resuspended in PBS and lysed ultrasonically. After centrifuging at 4 °C, 1500 g for 10 min, the supernatant was collected for measuring TNF-α, IL-2, IL-6, and IL-10. The experimental procedures were based on the instructions of the corresponding kits, including the Mouse TNF-α (Tumor Necrosis Factor Alpha) ELISA Kit (Elabscience Bionovation Inc., Wuhan, Hubei, China), the Mouse IL-2 ELISA Kit (Shanghai Enzyme-linked Biotechnology Co., Ltd., Shanghai, China), the Mouse IL-6 ELISA Kit and the Mouse IL-10 ELISA Kit (Jiangsu Meimian Industrial Co., Ltd., Yancheng, Jiangsu, China).

ROS measurement

The ROS measurement was performed using the Reactive oxygen species Assay Kit (Nanjing Jiancheng Bioengineering Institute, Nanjing, Jiangsu, China), which is based on the fluorescent probe 2, 7-dichlorodihydrofluorescein diacetate (DCFH-DA) to detect ROS. In brief, DCFH-DA was diluted by FBS-free DMEM at 1: 1000 to make the final concentration of 10 μM, which was used for incubating VSMCs for 20 min at 37 °C, 5% CO_2. Next, the unpenetrated DCFH-DA was washed out by the FBS-free DMEM for three times. The fluorescence was imaged under fluorescence microscope (Axio Observer 3, Carl Zeiss, Oberkochen, Baden-Württemberg, Germany) and the intensity was quantified by image J software.

Glutathione (GSH) and superoxide dismutase (SOD) detection

The cell supernatant was collected to determine the concentrations of GSH (the reduced type) and SOD by the reduced glutathione (GSH) assay kit and the superoxide dismutase (SOD) assay kit (WST-1 method) (Nanjing Jiancheng Bioengineering Institute Co., Ltd., Nanjing, Jiangsu, China), respectively, according to the manufacturer's protocols.

miRNA mimics addition

A 5 μL mmu-miR-17–5p mimics (MedChemExpress, Monmouth Junction, NJ, USA) was added to 120 μL FBS-free DMEM; and a 4 μL PolyFast was added to 121 μL FBS-free DMEM. The two mixtures were then gently mingled, and placed for 15 min at room temperature. The VSMCs in 1750 μL antibiotic free DMEM were incubated in the miRNA mixture in 6 well plates for 48 h. The cells were harvested for Western blotting.

Quantitative Real-Time PCR (qRT-PCR)

The total RNA of VSMCs was extracted via the SPARK easy Improved Tissue/Cell RNA Kit (Shandong Sparkjade Biotechnology Co., Ltd., Jinan, Shandong, China), followed by the reverse transcription using the miRNA 1st Strand cDNA Synthesis Kit (Vazyme Biotech Co., Ltd., Nanjing, Jiangsu, China). The primers were: reverse-miR-17–5p, GTCGTATCCAGTGCAGGGTCCGAGGTATTCGCACTGGA-TACGACCTACCT; reverse-U6-miRNA, GTCGTATCCAGTGCAGGGTCC-GAGGTATTCGCACTGGATACGACTGGAAC. qRT-PCR was performed based on a SYBR Green method, which uses the ChamQ Universal SYBR qPCR Master Mix (Vazyme Biotech Co., Ltd., Nanjing, Jiangsu, China) on an Eppendorf PCR System (Eppendorf AG, Hamburg, Germany), as described previously (Zhang et al., 2023). The miR-17–5p (Forward: GCGCAAAGTGCTTACAGTGC; Reverse: AGTGCAGGGTCCGAGGTATT). The internal reference U6 (Forward: GACACGCAAATTCGTGAAGC; Reverse: AGTGCAGGGTCCGAGGTATT) level was used as a baseline, the $2^{-\Delta\Delta CT}$ algorithm was employed to analyze the level of the target gene.

Statistics

The data was statistically analyzed using GraphPad Prism 8.0.2 and shown as mean±standard deviation (SD), based on at least three independent experiments. The p value for the significance of the difference was calculated by unpaired two-tailed Student's t-test, or one-way ANOVA for multiple groups with Dunnett's multiple comparisons test, which < 0.05 was significant.

Results

10-HDA inhibited the AngII-induced expression of TLR4 in VSMCs

To determine whether 10-HDA exerts effect on the expression of TLR4 in AngII-induced inflammatory VSMCs, the levels of TLR4 with 10-

HDA addition were relatively quantified. As is shown in **Fig. 1B&1C**, the levels of TLR4 in the VSMCs with AngII (0.1 μM, 1 μM and 10 μM) induction were significantly higher compared to that of the control ($p<0.05$, $p<0.01$, $p<0.001$) in a dose dependent manner. Using 10 μM AngII, 10-HDA significantly ($p<0.01$, $p<0.01$, $p<0.001$) inhibited the expressions of TLR4 does-dependently (1 mM, 2 mM and 4 mM) (**Fig. 1D&1E**). Compared to that of the AngII (10 μM)-treated VSMCs, the TLR4 inhibitor C34 (13 μM) significantly reduced the expressions of TLR4 ($p<0.001$), which had the similar effect as 10-HDA (4 mM) ($p<0.05$) (**Fig. 1F&1G**). Further, via immunostaining, 10-HDA (4 mM) significantly mitigated the AngII (10 μM)-induced fluorescent intensity of TLR4 in VSMCs ($p<0.05$) (**Fig. 1H&1I**). In all, 10-HDA had the potential to inhibit the expression of TLR4 in AngII-induced VSMC inflammation.

10-HDA reduced the AngII-stimulated up-regulation of SP1 and PPP6C in VSMCs

To identify the key proteins involving in 10-HDA regulating AngII-stimulated VSMC inflammation, the LC-MS/MS based proteomic analysis was performed. Among all the 9 groups, 36,887 peptides, as well as 4254 proteins, were identified. Compared to the control VSMCs, 168 proteins were significantly regulated with AngII (10 μM) stimulation, in which 105 were up-regulated whereas 63 were down-regulated (Fig. 2**A & Supplemental Table 1**). With 10-HDA (4 mM) addition, 77 proteins were significantly down-regulated, but 93 proteins were significantly up-regulated, in the AngII (10 μM)-stimulated VSMCs (Fig. 2**B & Supplemental Table 2**). Noticeably, 23 differentially expressed proteins were in both AngII *vs* control, and AngII+10-HDA *vs* AngII comparisons (Fig. 2**C**). The significantly up-regulated SP1 and PPP6C by AngII had the fold changes of 3.59 and 5.66, respectively. However, they were significantly down-regulated with the fold changes of 1.77 and 17.93, respectively, treated both by 10-HDA and AngII. Their comparisons in the form of violin plot were shown in **Fig. 2D&2E**. Such fact suggested SP1 and PPP6C may be the crucial regulators associated with the effect of 10-HDA on AngII-mediated VSMC inflammation. Further, by Western blotting analysis, the trends of level variations of the two proteins were similar. The significantly increased levels of SP1 ($p<0.05$) and PPP6C ($p<0.05$) by AngII (10 μM) could be significantly inhibited ($p<0.05$, $p<0.01$) by 10-HDA (4 mM) (Fig. 2**F, 2G&2H**). In the PPI network analysis, 13 subnetworks were constructed by the 23 proteins. SP1, implicated in the Subnetwork 3, had the high degree of 28. PPP6C was in the Subnetwork 11 with the degree of 4 (**Fig. 2I**). The evidence indicated that SP1 and PPP6C, particularly SP1, were the important hub nodes in the networks. Through immunostaining, the fluorescent intensity to reflect SP1 level in VSMCs was significantly enhanced by AngII (10 μM) ($p<0.01$), which was significantly reduced with 10-HDA (4 mM) supplementation ($p<0.05$) (**Fig. 2J&2K**).

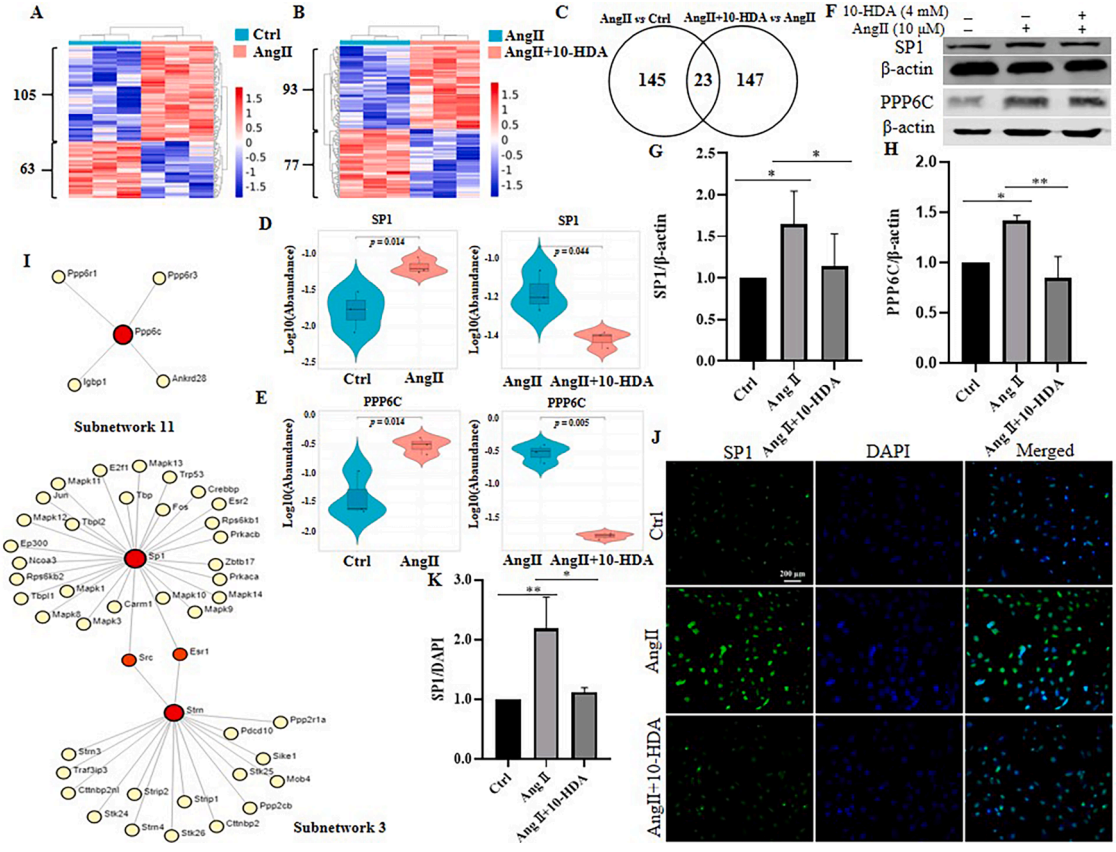

Fig. 2. 10-HDA prevents the up-regulations of SP1 and PPP6C that are stimulated by AngII in VSMCs. A & B Heat maps display the differentially expressed proteins in AngII (10 μM) *vs* control, and AngII (10 μM) + 10-HDA (4 mM) *vs* AngII (10 μM) VSMCs from proteomic analysis. C Venn diagram shows the numbers, including the common ones, of the differentially expressed proteins in the two comparative groups. D & E Violin charts exhibit the changes of SP1 and PPP6C levels implicated in the heat map data. F Western blots represent the expressions of SP1 and PPP6C mediated by AngII (10 μM) and AngII (10 μM) + 10-HDA (4 mM) in VSMCs. G & H Relative quantification for SP1 and PPP6C levels normalized to β-actin. I PPI networks denote the connections of SP1 and PPP6C to other nodes. Red dots represent the nodes that are the differentially expressed proteins, whose areas symbolize their degrees within the networks. J Immuno-staining of SP1 in VSMCs that are treated by AngII (10 μM) or AngII (10 μM) + 10-HDA (4 mM), in which scale bar is 200 μm. K The quantitative florescent intensity for SP1/DAPI ratio. All data are shown as mean ± SD (n=3); *$p<0.05$, **$p<0.01$.

10-HDA modulated the AngII-mediated phosphorylation of ERK1/2, TAK1, and NF-κB p65 in VSMCs

To disclose the role of 10-HDA in modulating signaling pathways that underlie the AngII-mediated VSMC inflammation, the Signaling Network was generated by the 23 proteins, followed by the determination of the phosphorylation of ERK1/2, TAK1, and NF-κB p65 via Western blot analysis. In the 3 generated subnetworks, Subnetwork 1 displayed that the hub node SP1 interacted with mitogen-activated protein kinases (MAPKs), and ERK1/2 (Fig. 3**A**). The Western blotting showed that phosphorylated ERK1/2 ($p<0.05$) was significantly activated by AngII (10 μM). However, with the addition of 10-HDA (4 mM), such level was significantly declined ($p<0.01$) (**Fig. 3B&3C**). The phosphorylation of TAK1 was also significantly activated by AngII (10 μM) ($p<0.05$) but significantly remedied by 10-HDA (4 mM) ($p<0.01$) (**Fig. 3B&3D**). The phosphorylation of NF-κB p65 had the similar trend to those of ERK1/2 and TAK1 (**Fig. 3B&3E**). The data indicated that 10-HDA could intervene in the MAPK-related VSMC inflammation. Moreover, the level change of MyD88 resembled these phospho-proteins in VSMCs by AngII and 10-HDA (**Fig. 3B&3F**).

10-HDA might interfere with the combination of TLR4 and LPS

To elucidate the mode of 10-HDA interacting with TLR4, the molecular docking strategy for the two molecules was applied. Each docking generated four poses, in which Pose 1 had the best score. The docking scores based on the three performances were -3.8/-3.7/-3.7 (Pose 1), -3.7/-3.7/-3.6 (Pose 2), -3.3/-3.6/-3.5 (Pose 3) and -3.2/-3.3/-3.5 (Pose 4). Interestingly, Serine (A:413), a possible site to combine LPS, was engaged in all 12 poses by conventional hydrogen bond, unfavorable acceptor-acceptor, or van der Waals with 10-HDA, indicating that 10-HDA might block the combination of TLR4 and LPS in the Serine (A:413) position. Specifically, the conventional hydrogen bond could occur between Serine (A:413) and the hydrogen atom of hydroxyl group or carboxyl group of 10-HDA (Fig. 4**A,** Fig. 4**B & Supplemental Fig. 1**). The unfavorable acceptor-acceptor might exist between Serine (A:413) and the oxygen atom of hydroxyl group of 10-HDA (Fig. 4**C**). The predicted van der Waals between Serine (A:413) and 10-HDA were displayed in Fig. 4**D & Supplemental Fig. 2**. Through Western blot, TLR4 was significantly up-regulated ($p<0.05$) by LPS (1 μg/mL) in VSMCs. However, the activation of TLR4 by LPS was significantly inhibited ($p<0.01$) with 10-HDA addition (4 mM) (Fig. 4**E&**4**F**). Such effect of 10-HDA to reduce the abundance of TLR4 in LPS-treated VSMCs was also evidenced by immuno-staining (Fig. 4**G&**4**H**).

10-HDA regulated the expressions of SP1, as well as the phosphorylation of ERK1/2, TAK1, and NF-κB p65, mediated by LPS in VSMCs

To unravel the mode of 10-HDA to engage in LPS-mediated VSMC activity, Western blot was applied to determine the levels of SP1, PPP6C, as well as phosphorylated ERK1/2, TAK1, and NF-κB p65. As was shown in Fig. 5**A&5B**, the significant down-regulation of SP1 by LPS (1 μg/mL) ($p<0.01$) was significantly rescued in case of 10-HDA (4 mM) treatment ($p<0.01$). The level of PPP6C had insignificant change with the addition of LPS (1 μg/mL) ($p>0.05$). In such occasion, 10-HDA (4 mM) did not significantly alter the PPP6C level ($p>0.05$) (Fig. 5**A&5C**). Resembling AngII, treatment by LPS (1 μg/mL) significantly boosted the phosphorylation of ERK1/2 ($p<0.01$), TAK1 ($p<0.01$) and NF-κB p65 ($p<0.01$). Accordingly, 10-HDA (4 mM) significantly reversed their phosphorylated levels ($p<0.01$; $p<0.05$; $p<0.05$) (Fig. 5**D,** 5**E,** 5**F&**5**G**). 10-HDA (4

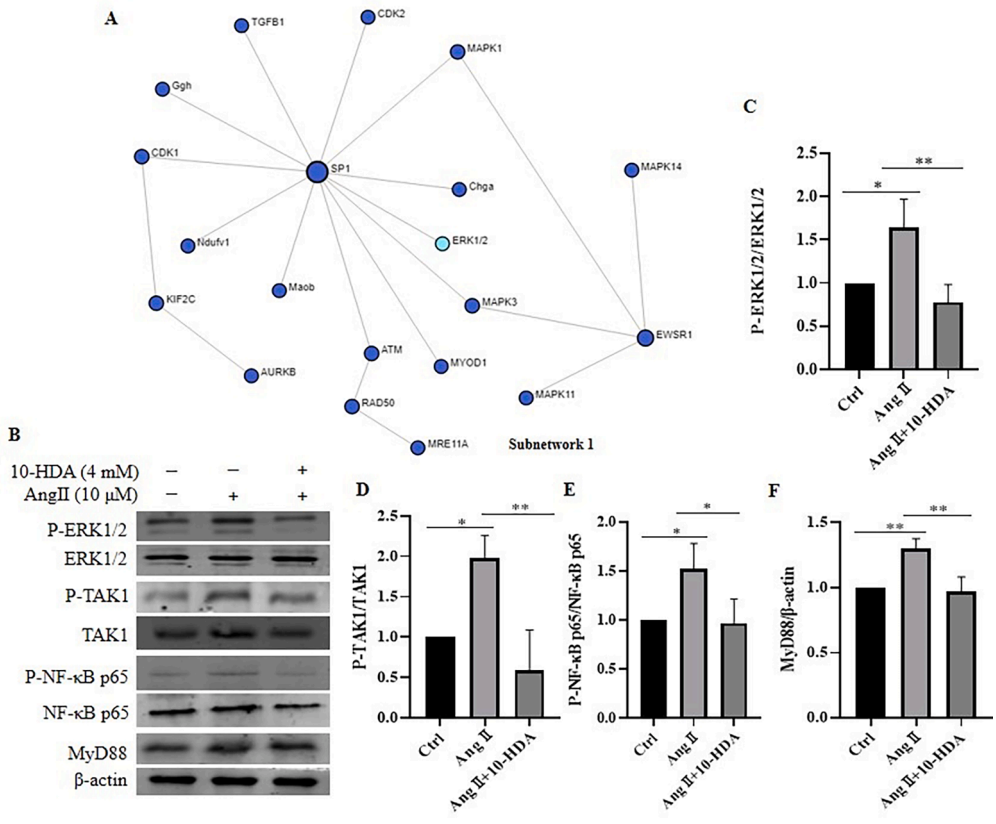

Fig. 3. 10-HDA attenuates the enhanced levels of P-ERK1/2, P-TAK1, P-NF-κB, and MyD88 by AngII in VSMCs. A Signaling network shows the links between SP1 and signaling pathway components. The areas of the nodes indicate the degrees of the nodes within the network. B Western blots represent the level variations of P-ERK1/2, P-TAK1, P-NF-κB p56, and MyD88 by AngII (10 μM) and AngII (10 μM) + 10-HDA (4 mM) in VSMCs. C, D, E & F Comparisons of P-ERK1/2, P-TAK1, P-NF-κB p56, and MyD88 levels normalized to T-ERK1/2, T-TAK1, T-NF-κB p56, and β-actin. All data are shown as mean ± SD ($n=3$); *$p<0.05$, **$p<0.01$.

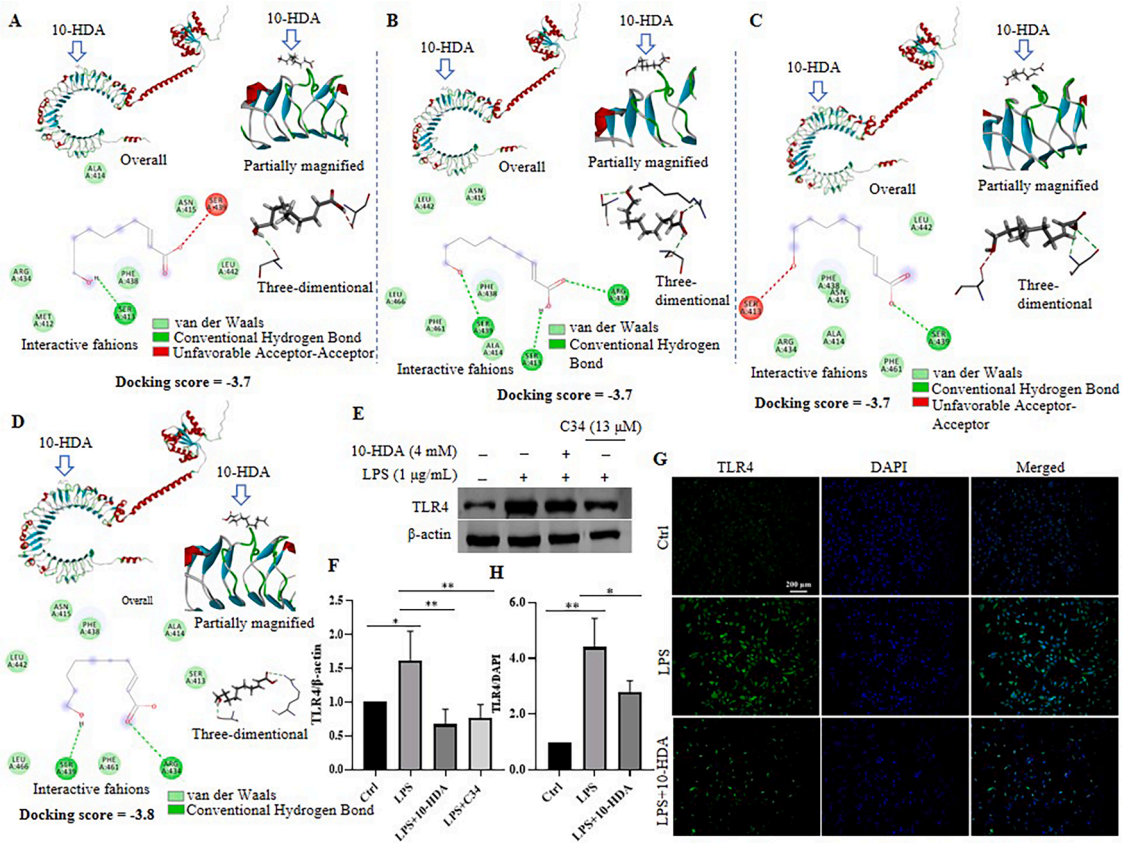

Fig. 4. 10-HDA could block the bind of TLR4 and LPS. A, B, C & D Overall views, partially magnified views, interactive fashions of 10-HDA atoms-TLR4 amino acids, and three-dimentional visulizations of the predicted interactions of 10-HDA and TLR4 in the poses from the molecular docking. E Representative Western blots indicate the changes of TLR4 level by 10-HDA (4 mM) and C34 (13 μM) in VSMCs with LPS (1 μg/mL) stimulation. F Intensity comparisons of TLR4 normalized to β-actin in different VSMC groups. G Representative images of VSMCs with the treatment of LPS (1 μg/mL) or LPS (1 μg/mL) + 10-HDA (4 mM) stained by TLR4 and DAPI (scale bar is 200 μm). H Differences of TLR4/DAPI fluorescent intensity ratios in VSMCs with LPS (1 μg/mL) or LPS (1 μg/mL) + 10-HDA (4 mM) treatment. All data are shown as mean ± SD (n=3); *p<0.05, **p<0.01.

mM) also significantly hampered (p<0.05) the significant enhancement of MyD88 expression by LPS (1 μg/mL) (p<0.05) in VSMCs (Fig. 5**D**&5**H**).

10-HDA decreased TNF-α, IL-2 and IL-6 but increased IL-10 in AngII- or LPS-treated VSMCs

To find whether 10-HDA could exert effects on AngII- or LPS-induced VSMC inflammation, the key cytokines, including TNF-α, IL-2, IL-6 and IL-10, were quantified. The proinflammatory cytokine TNF-α (p<0.0001), IL-2 (p<0.0001) or IL-6 (p<0.0001) in VSMCs was significantly up-regulated by AngII (10 μM), which was impeded in the presence of 10-HDA (1 mM and 4 mM). The difference between AngII and AngII+10-HDA (1 mM) was insignificant for TNF-α (p>0.05) or IL-2 (p>0.05) but significant for IL-6 (p<0.05). In contrast, the differences between AngII and AngII+10-HDA (4 mM) were all significant for the three cytokines (p<0.001; p<0.001; p<0.0001) (Fig. 6**A**, 6**C**&6**E**). Similarly, the significant elevation of TNF-α (p<0.0001), IL-2 (p<0.0001) or IL-6 (p<0.0001) level by LPS (1 μg/mL) was mitigated in response to 10-HDA (1 mM and 4 mM) but with insignificant differences (p>0.05 for TNF-α and IL-2) exclusive of IL-6 (p<0.05) when 10-HDA was in low dose (1 mM). The high dose of 10-HDA (4 mM) contributed to the significant differences for all parameters (p<0.001; p<0.01; p<0.001) (Fig. 6**B**, 6**D**&6**F**). On the contrary, the anti-inflammatory cytokine IL-10 was significantly down-regulated by AngII (10 μM) (p<0.0001) or LPS (1 μg/mL) (p<0.01), which was significantly prevented by high dose of 10-HDA (4 mM) (p<0.001; p<0.05) but insignificantly by low dose of 10-HDA (1 mM) (p>0.05) (Fig. 6**G**&6**H**). Taken together, 10-HDA had the inhibitory impact on VSMC inflammation activated by AngII or LPS.

10-HDA decreased ROS but increased GSH and SOD levels in AngII- or LPS-administrated VSMCs

To reveal the mechanism underlying 10-HDA regulating inflammation, ROS, along with the anti-oxidant GSH and SOD, were analyzed in VSMCs. The level of ROS was significantly augmented by AngII (10 μM) (p<0.001) or LPS (1 μg/mL) (p<0.05) in VSMCs. With the administration of 10-HDA of 1 mM, it was significantly (p<0.01) or insignificantly (p>0.05) down-scaled. When 10-HDA was in the dose of 4 mM, difference between AngII and AngII+10-HDA (p<0.001) or that between LPS and LPS+10-HDA (p<0.05) was significant (Fig. 7**A**, 7**B**, 7**C**&7**D**). The contents of GSH (p<0.0001) and SOD (p<0.05), significantly dropped with AngII (10 μM) induction, were significantly (p<0.01) and insignificantly (p>0.05) saved by low dose (1 mM) of 10-HDA. Comparatively, they were both significantly (p<0.0001; p<0.01) saved by the high dose (4 mM) treatment (Fig. 7**E**&7**G**). In the VSMCs with LPS (1 μg/mL) stimulation, the effect of 10-HDA on GSH and SOD was similar. The significantly downgraded GSH (p<0.0001) and SOD (p<0.01) levels by LPS were significantly (p<0.05) and insignificantly (p>0.05) compromised in case 1mM 10-HDA was added, while the differences for both GSH and SOD were significant (p<0.01; p<0.01) when 4 mM 10-HDA was used (Fig. 7**F**&7**H**). Therefore, 10-HDA could reduce ROS in VSMCs via fortifying the anti-oxidant activity.

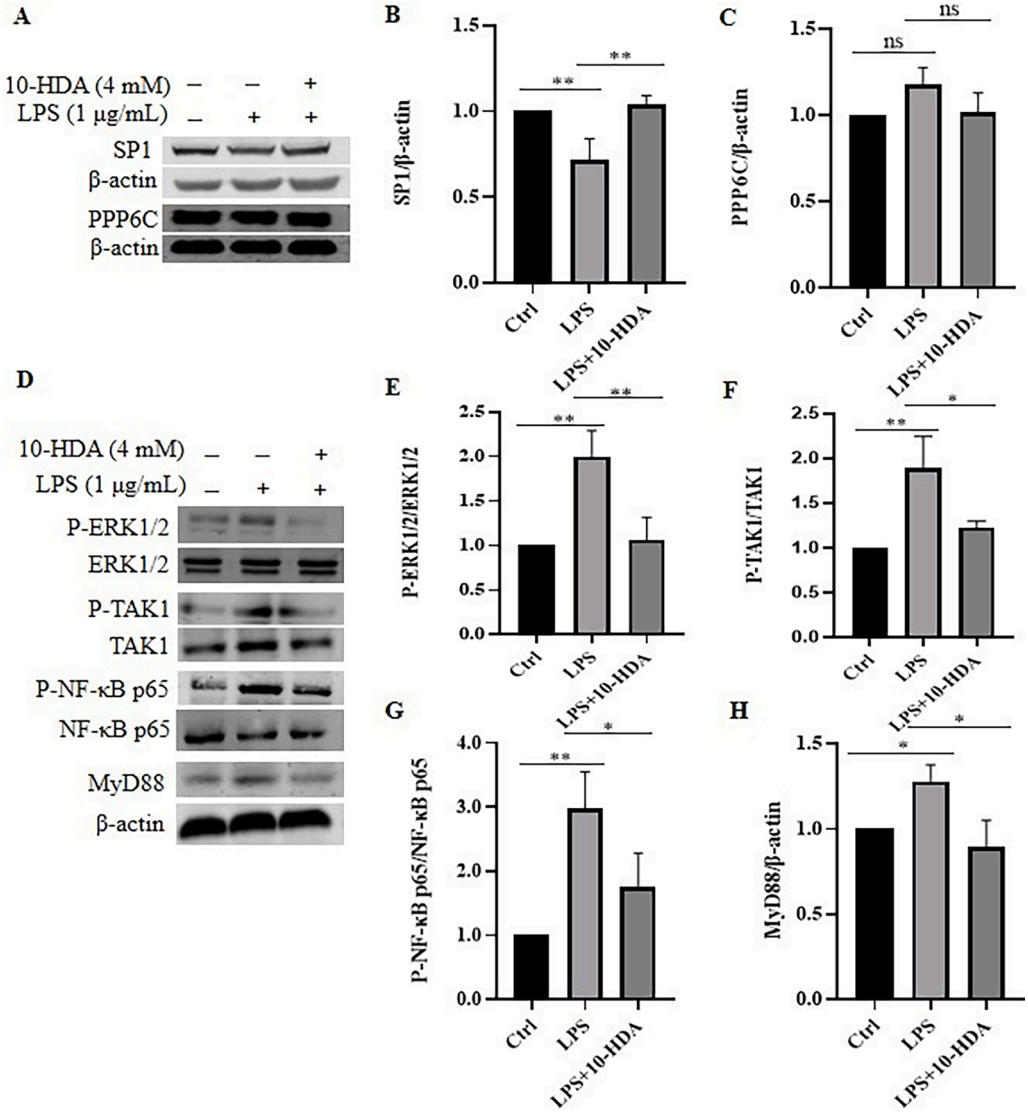

Fig. 5. 10-HDA decelerates the elevated expressions of P-ERK1/2, P-TAK1, P-NF-κB, and MyD88 by LPS in VSMCs. A Western blots represent the levels of SP1 and PPP6C regulated by LPS (1 μg/mL) or that with 10-HDA (4 mM). B & C Column charts indicate the comparison of SP1 or PPP6C normalized to β-actin between control, LPS (1 μg/mL) and LPS (1 μg/mL) + 10-HDA (4 mM) treated VSMCs. D Representative Western blots show the expression variations of P-ERK1/2, P-TAK1, P-NF-κB p56, and MyD88 from LPS (1 μg/mL) or LPS (1 μg/mL) + 10-HDA (4 mM) treatment. E, F, G & H Densitometry analysis for the phospho-proteins normalized to their Total-counterparts, or the MyD88 to β-actin. All data are shown as mean ± SD (n=3); *p<0.05, **p<0.01, *ns*: no significant difference.

10-HDA promoted the expression of miR-17–5p in VSMCs with AngII or LPS addition

To expound whether 10-HDA fine-tunes VSMC inflammation, the Gene-miRNA Interactions network was constructed by the 23 differentially expressed proteins. As was shown in Fig. 8**A**, miR-17–5p connected SP1 and PPP6C, the nodes with the first and the fourth highest degrees (136 and 101, respectively) in the network. As for miRNAs in the network, miR-17–5p had the highest degree of 17. Such results suggested SP1, PPP6C and miR-17–5p may be the key regulators therein. Through TargetScan prediction, the 3′ UTRs of SP1 and PPP6C mRNAs had the complementary sites for miR-17–5p (Fig. 8**B**), indicating they could be the targeted genes of miR-17–5p. Furthermore, Western blotting analysis showed that the expressions of SP1 (p<0.01) and PPP6C (p<0.0001) were significantly lowered by miR-17–5p mimics (5 μL) (Fig. 8**C,** 8**D&**8**E**). In the VSMCs treated by AngII (10 μM) (p<0.0001) or LPS (1 μg/mL) (p<0.0001), miR-17–5p was significantly down-regulated. However, in such occasion, the expression of miR-17–5p was significantly promoted by 10-HDA (4 mM) (p<0.0001; p<0.0001) (Fig. 8**F&**8**G**). In summary, miR-17–5p may be involved in the modulation of VSMC inflammation by 10-HDA.

Discussion

AngII stimulates TLR4 expression in VSMCs, which initiates inflammatory responses, and may result in a broad range of vascular diseases thereafter. In the present study, 10-HDA is able to inhibit the AngII-induced up-regulation of TLR4 in VSMCs in a dose-dependent manner. Such evidence is in accordance with the fact that 10-HDA can interact with TLR4, implicating that TLR4 could be a potential target of 10-HDA in vascular system. As a membranous receptor, TLR4 may have a subset of downstream effector molecules. Here, by virtue of proteomic screen, the expression of SP1 is suppressed by 10-HDA from the AngII-induced VSMCs. SP1 is a famous member of SP-family of transcription factors. The transcription of genes whose promoters contain putative CG-rich Sp-binding sites can be activated by SP1 within cells (Vizcaíno et al., 2015). The effect of AngII on SP1 as in our study corroborates with earlier studies in cardiac fibroblasts (Li et al., 2015). Notably, SP1

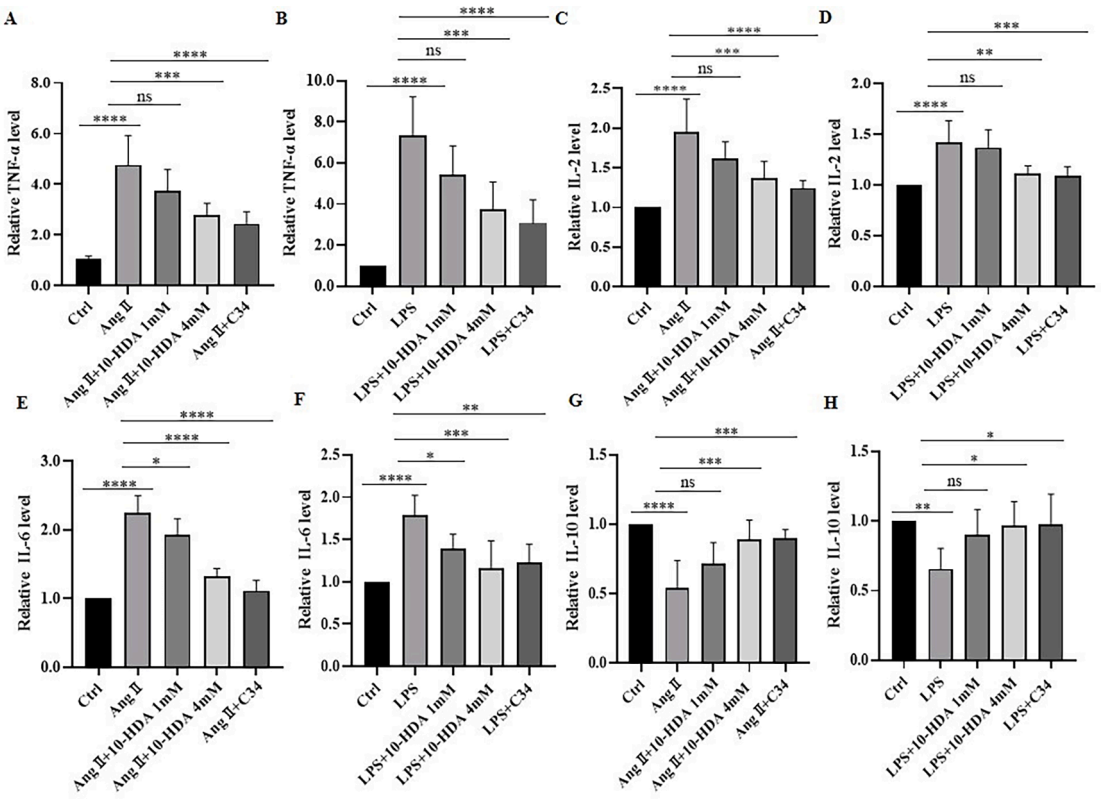

Fig. 6. 10-HDA regulates inflammatory cytokines in AngII- or LPS-treated VSMCs. A & B Column charts show the differences of TNF-α levels in control, AngII (10 μM)- or LPS (1 μg/mL)-treated VSMCs and that with 10-HDA (1 mM and 4 mM) or C34 (13 μM). C & D Comparisons of IL-2 levels between different VSMC groups. E & F Relative quantification for IL-6 levels in those groups. G & H Quantitative analysis for IL-10 levels. All data are shown as mean ± SD (n=6); *p<0.05, **p<0.01, ***p<0.001, ****p<0.0001, and ns for no significance.

transcriptional regulatory element is present within, and important in the regulation of, the murine TLR4 promoter (range -750 bp to -250 bp) (Wasiluk et al., 2006). On the other hand, the direct inhibition of TLR4 led to the suppressed expression of SP1 (Zhang et al., 2020), indicating their closely and mutually regulatory relationship. Therefore, 10-HDA may possibly function by the suppression of TLR4 to attenuate SP1. Besides being a regulator of tumor-associated genes (Beishline and Azizkhan-Clifford, 2015), SP1 was identified to be a key player in the pathogenesis of atherosclerosis, which involves in the development of inflammation and VSMC proliferation. It was therefore considered the therapeutic target of atherosclerosis (Jiang et al., 2022). The ability of 10-HDA to attenuate AngII-induced elevation of SP1 in VSMCs makes 10-HDA a promising agent to alleviate VSMC inflammation-derived symptoms.

PPP6C is also screen to be down-regulated by 10-HDA from AngII stimulation in VSMCs. The expression of PPP6C can be up-regulated in glioma tissues (Guo et al., 2014) and cervical cancer (Zhu et al., 2020). Knockdown of PPP6C suppresses the proliferation of acute myeloid leukemia cells (Bao et al., 2021). Unlike SP1, the knowledge about the role of PPP6C in VSMCs is rare. However, there are still some clues relating TLR4 with PPP6C. PPP6C is a catalytic subunit of serine/threonine phosphatase 6, which could be in response to IL-2 receptor stimulation (Filali et al., 1999). IL-2, a pro-inflammatory cytokine, is able to provoke TLR4 surface expression on human peripheral blood monocytes (Mita et al., 2002). Moreover, IL-2 could also be modulated by TLR4. For instance, ethanol extract of *Anacyclus pyrethrum* root suppresses the expression of TLR4 that plays a similar role to the TLR4 antagonist E5564, and results in the decrease of IL-2 in cough variant asthma (Zheng et al., 2023). A natural compound *Coriolus versicolor* administration reduces the activation of the TLR4-related pathway and the level of IL-2 in the autoimmune myocarditis model (Interdonato et al., 2023). In VSMCs, IL-2 can somewhat enhance the Ca^{2+} influx and the stimulation of DNA synthesis induced by AngII (Nabata et al., 1997). Therefore, the fact that IL-2 is involved in the responsiveness to AngII might be contributive to the PPP6C activity. The involvement of 10-HDA to regulate PPP6C in AngII-stimulated VSMCs may help enhance the knowledge regarding TLR4 pathway, which needs further investigations.

In the framework of molecular docking, 10-HDA might insert in the sites that TLR4 and LPS combine. Serine (A:413) may be the major binding site for TLR4 and LPS as reported earlier (Ohto et al., 2012). In the present analysis, Serine (A:413) could interact with the hydrogen atom of hydroxyl group or carboxyl group in 10-HDA through conventional hydrogen bond, and the oxygen atom of hydroxyl group in 10-HDA via unfavorable acceptor-acceptor. Moreover, Serine (A:413) and 10-HDA might be interactive by van der Waals force. Therefore, the mode of 10-HDA to influence TLR4 activity may be dependent on its interference with TLR4 and LPS combination. When challenged by LPS, the SP1 expression can be down-regulated in many cell types such as cardiomyocyte (Chen et al., 2021). In VSMCs, similar effect of LPS on SP1 was observed and the reduction was reversed by 10-HDA, indicating 10-HDA could engage in the LPS activity. Although both AngII and LPS are able to induce inflammation, the underlying mechanisms may be different. In this study, their regulations on SP1 are not the same. In addition, PPP6C is not affected by LPS, as well as 10-HDA in the context of LPS in the present data, further revealing that the styles of 10-HDA modulating VSMC inflammation through TLR4 are partly distinct with varied stimulants.

In PPI network analysis for the 23 differentially expressed proteins commonly in the AngII *vs* control and the AngII+10-HDA *vs* AngII groups, SP1 highly interacts with MAPK signaling pathway. In fact, their relationships were documented in early years (Kim et al., 2012).

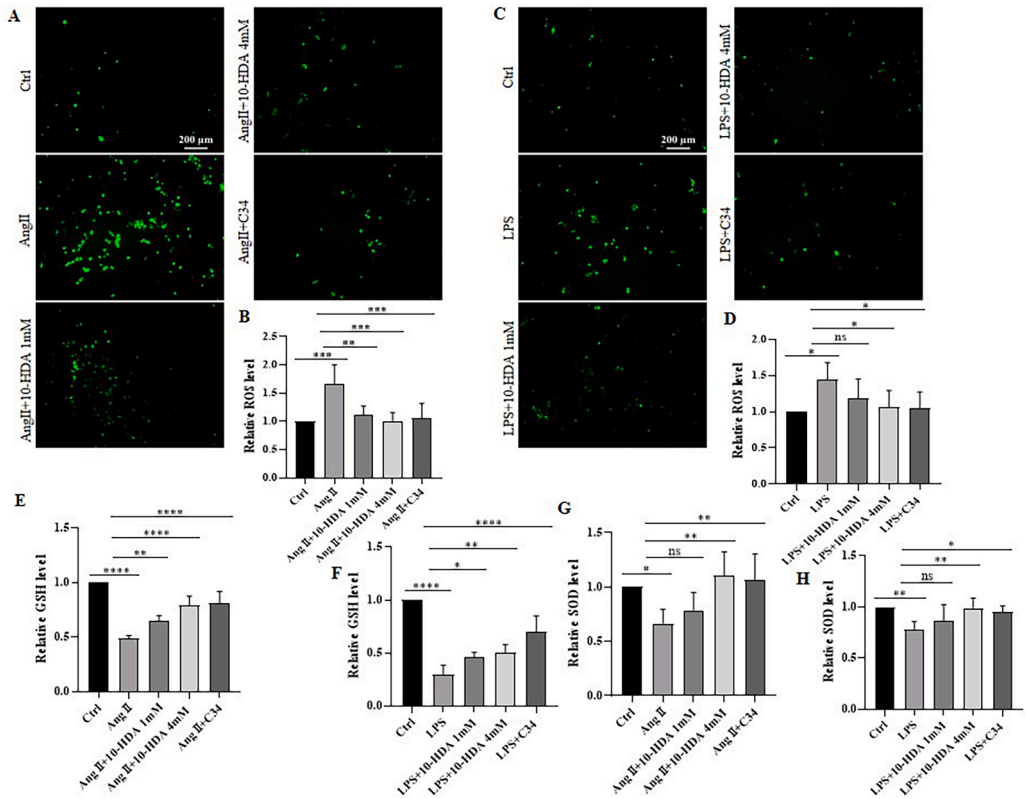

Fig. 7. 10-HDA reduces AngII- or LPS-induced ROS in VSMCs. A Images show fluorescence in VSMCs probed by DCFH-DA, which indicates ROS level. The scale bar is 200 μm. B Quantification for the fluorescent intensities in VSMCs with AngII (10 μM), AngII (10 μM) + 10-HDA (1 mM and 4 mM), or AngII (10 μM) + C34 (13 μM). C Florescence visualization of DCFH-DA in VSMCs represents ROS content. The scale bar is 200 μm. D Comparisons of ROS levels for different VSMC groups. E & F Quantitative analysis for GSH in VSMCs treated by 10-HDA (1 mM and 4 mM) or C34 (13 μM) with AngII (10 μM) and LPS (1 μg/mL) induction, respectively. G & H Relative quantification for SOD in 10-HDA (1 mM and 4 mM)- or C34 (13 μM)-administrated VSMCs respectively stimulated by AngII (10 μM) and LPS (1 μg/mL). All data are shown as mean ± SD (n=6); *p<0.05, **p<0.01, ***p<0.001, ****p<0.0001, and ns for no significance.

Meanwhile, P-ERK1/2 is positively correlated with TLR4 activity (Park et al., 2021). As is well-known, AngII activates P-ERK1/2 level in VSMCs (Sousa-Lopes et al., 2020), which is also shown in our data. The VSMCs stimulated by LPS have a boosted P-ERK1/2 level, as evidenced previously (Chen et al., 2022a) and here. As the inhibition of ERK1/2 phosphorylation can attenuate inflammation in some pathogenic conditions (Li et al., 2021), 10-HDA reducing the level of P-ERK1/2 induced by AngII or LPS suggests that 10-HDA could remedy VSMC inflammation challenged by AngII via TLR4/SP1-related cascades.

Besides P-ERK1/2, the enhancement of P-TAK1 and P-NF-κB p65 (an important component of NF-κB) induced by AngII or LPS in VSMCs can be moderated by 10-HDA. MyD88, a central node of inflammatory pathways that connects TLRs to a variety of kinases (Deguine and Barton, 2014), has the similar alterations when exposes to AngII or LPS, as well as that with 10-HDA. Activation of TLR4-MyD88-TRAF6-TAK1 pathway is necessary for NF-κB Activation (He et al., 2016). In VSMCs, TLR4, TAK1 and NF-κB co-work as a signaling pathway (Meng et al., 2019). Hence, the coordination of P-TAK1, P-NF-κB p65 and MyD88 essentially contributes to the TLR4 signaling. Such downstream kinases of TLR4 influenced by 10-HDA further indicates 10-HDA's capability to reduce inflammatory responses in VSMCs via interacting with TLR4.

VSMC can be shifted from quiescent contractile phenotype to a pro-inflammatory phenotype, characterized by the secretion of inflammatory cytokines (Wang et al., 2022), some of which are inducible by AngII or LPS (de Lima et al., 2019; Ye et al., 2018). In the present study, the TNF-α, IL-2 and IL-6 production in AngII- or LPS-challenged VSMCs is inhibited by 10-HDA. The pro-inflammatory cytokines always act as the stimulants for crucial signaling pathways, including P-ERK1/2, P-TAK1 and P-NF-κB p65 (Kojima et al., 2005; Lee et al., 2019; Wang et al., 2000; Yu et al., 2000). They are also the determinants for ROS production (Mehra et al., 2005; Sprague and Khalil, 2009). As is widely reported, the ROS generation can be derived from the cells in innate immune system to kill pathogens, and is increased by long-term inflammation process (Agita and Alsagaff, 2017). The excessive ROS cause oxidative stress and thereby contribute to a wide range of cell dysfunctions and disorders, such as cardiovascular disease (Satoh et al., 2010) and chronic kidney disease (Daenen et al., 2019). Therefore, abating ROS induced damage could be beneficial to cell and body health. Interestingly, ROS biogenesis can be regulated by TLR4 (Dong et al., 2021). The inhibition of TLR4 attenuates vascular oxidative stress (Carrillo-Sepulveda et al., 2015). 10-HDA decreases the ROS production in VSMCs promoted by AngII or LPS may be due to its ability to increase GSH and SOD. Concurrently, IL-10, an anti-inflammatory cytokine that limits immune response to pathogens and prevents host damage (Saraiva and O'Garra, 2010), protects against AngII-induced oxidative stress and vascular dysfunction (Didion et al., 2009). Hence, through recuperating IL-10 levels inhibited by AngII or LPS could be the mode of 10-HDA to reduce VSMC inflammation.

The endogenously originated non-coding miRNAs, having the lengths of 20–25 nt (usually 22 nt), can negatively regulate their target genes through incomplete complementarity between the seed region of miRNAs and the 3′UTR of mRNAs, thus fine-tune multiple cellular processes (Lewis et al., 2005; Zhou et al., 2012). miR-17–5p is a fundamental member of miR-17/92 cluster, which engages in immunity (Kuo et al., 2019), cancers (Zhao et al., 2022), obesity, kidney diseases, cardiovascular diseases, and diabetes (Ejaz et al., 2023). In VSMCs, miR-17–5p inhibits proliferation and migration under the stimulation of platelet-derived growth factor-BB by targeting homeobox B13 (Yu et al., 2021), and promotes alkaline phosphatase activity, which is critical for

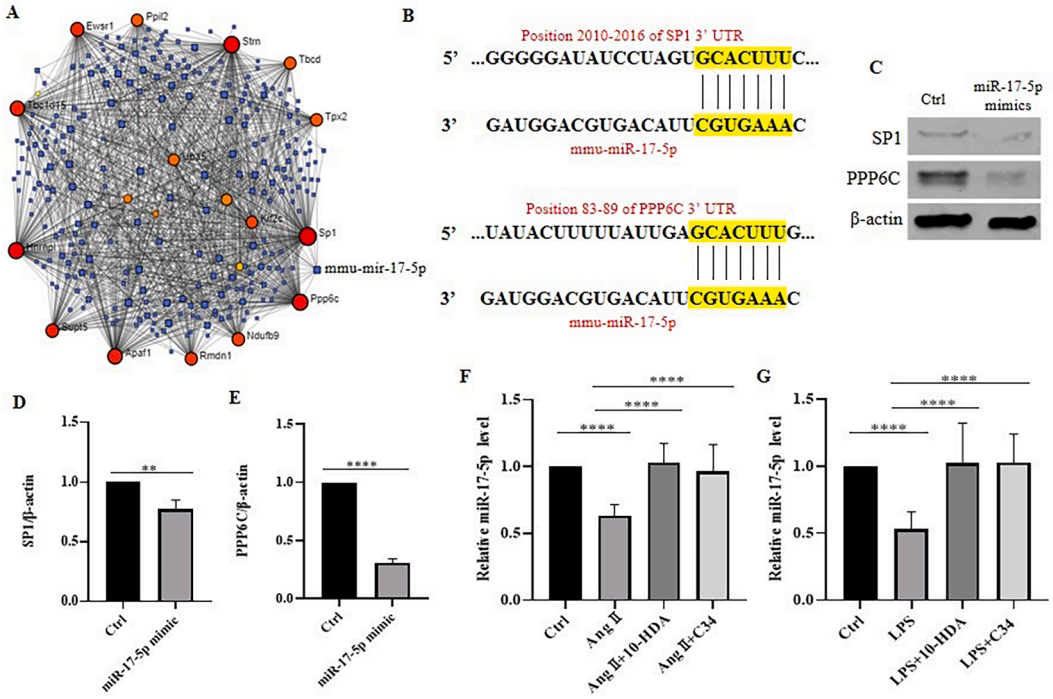

Fig. 8. miR-17–5p involves in the regulation of 10-HDA for VSMCs. A Network constructed by the differentially expressed proteins predicts the interactions between miRNAs and genes, which are represented by squares and circles, respectively. The areas of the nodes indicate their degrees within the network. B Complementary sites for miR-17–5p and 3′UTR of SP1 or PPP6C mRNA. The highlighted sequences are the binding sites. C Western blots show the expressions of SP1 and PPP6C affected by the addition of miR-17–5p mimics (5 μL) in VSMCs. D & E Relative quantification of SP1 and PPP6C normalized to β-actin, respectively. F Relative miR-17–5p levels in VSMCs of control, AngII (10 μM), AngII (10 μM) + 10-HDA (4 mM), and AngII (10 μM) + C34 (13 μM) groups. G Relative miR-17–5p levels in VSMCs of control, LPS (1 μg/mL), LPS (1 μg/mL) + 10-HDA (4 mM), and LPS (1 μg/mL) + C34 (13 μM) groups. All data are shown as mean ± SD (n=6); $^{**}p<0.01$, $^{****}p<0.0001$.

vascular calcification, by targeting ankylosis protein homolog (Shi et al., 2022). The evidences suggest miR-17–5p is a key regulator for VSMC function. Notably, TLR4 is also a target of miR-17–5p, which is reflected in the PC_{12} cells that the expressions of miR-17–5p and TLR4 are down- and up-regulated with oxygen-glucose deprivation and reperfusion, respectively (Suo and Wang, 2022). Nevertheless, by miRNA-Gene network analysis in the present data, miR-17–5p is shown to connect SP1 and PPP6C, indicating that the two key nodes may be the targets of miR-17–5p in VSMCs. In fact, the miR-17–5p mimics inhibit the expressions of the two proteins. Interestingly, 10-HDA guards against the

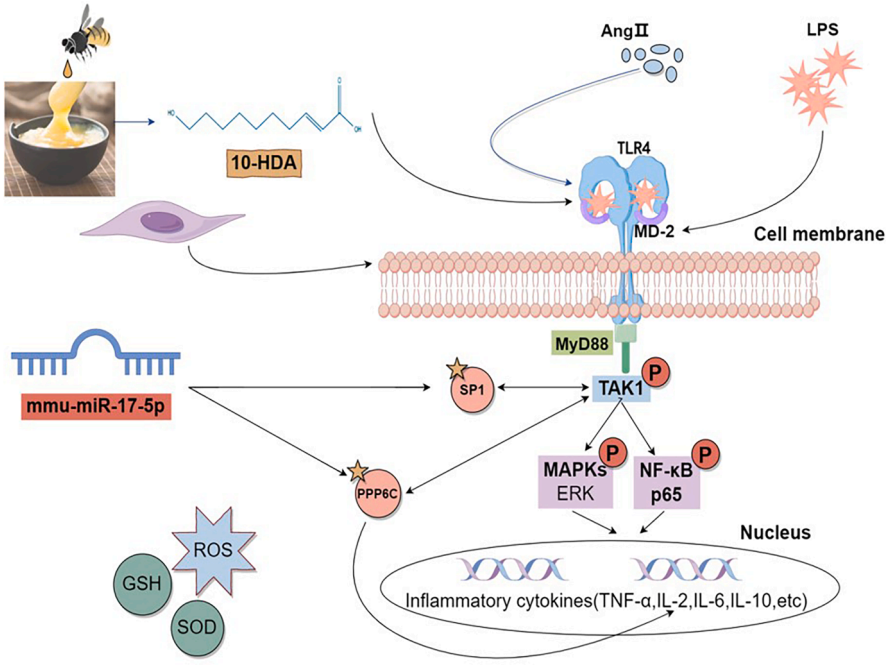

Fig. 9. The pictorial summary of the molecular mechanism underlying VSMC inflammatory regulation by 10-HDA.

miR-17–5p level from AngII or LPS challenge, the novel exploration could expand the knowledge of 10-HDA and miRNA relationship. Here, miR-17–5p is identified as a crucial miRNA in mediating VSMC inflammation via TLR4 pathway.

In conclusion, 10-HDA could interact with TLR4 to block TLR4 and LPS binding. The activation of TLR4 by AngII or LPS in VSMCs is attenuated by 10-HDA. SP1 and PPP6C may be the two pivotal proteins associated with 10-HDA regulation. In the presence of AngII or LPS, the activated phosphorylation of ERK1/2, TAK1 and NF-κB, along with the enhanced levels of TNF-α, IL-2 and IL-6, can be decreased by 10-HDA. 10-HDA is capable of increasing IL-10, GSH and SOD whereas reducing ROS thereof. All data indicate that 10-HDA has the ability to inhibit VSMC inflammation by modulating a set of signaling pathways through TLR4. In addition, miR-17–5p may play an important role in the regulative process with regard to 10-HDA. Our present work establishes the links between 10-HDA and VSMC inflammation by a set of participating molecules (Fig. 9), which will cast light on the utilization of 10-HDA in the perspective of VSMC inflammation-related vascular abnormality. Our next work would include the *in vivo* study to test the effect of 10-HDA on inflammatory vascular diseases.

Funding

This work is supported by the Open Project Program of National Engineering Research Center of Wheat and Corn Further Processing, Henan University of Technology (No. NL2023004), the Cultivation Programme for Young Backbone Teachers in Henan University of Technology (No. 21420168).

CRediT authorship contribution statement

Feng Jia: Conceptualization, Investigation, Formal analysis, Writing – review & editing, Supervision. **Yongqing Wang:** Investigation, Formal analysis, Writing – review & editing. **Zhiqiang Chen:** Investigation, Formal analysis. **Jingxian Jin:** Investigation, Formal analysis. **Lei Zeng:** Methodology, Writing – review & editing. **Li Zhang:** Methodology, Project administration. **Huaijian Tang:** Investigation, Formal analysis. **Yanyan Wang:** Investigation, Formal analysis. **Pei Fan:** Conceptualization, Methodology, Investigation, Formal analysis, Writing – original draft, Supervision.

Declaration of competing interest

The authors declare that they have no known competing financial interests or personal relationships that could have appeared to influence the work reported in this paper.

Acknowledgement

We thank Beijing Qinglian Biotech Co., Ltd., Beijing, China, for the LC-MS/MS analysis; and Figdraw for generating the graphical mechanism.

Supplementary materials

Supplementary material associated with this article can be found, in the online version, at doi:10.1016/j.phymed.2025.156534.

References

Agita, A., Alsagaff, M.T., 2017. Inflammation, immunity, and hypertension. Acta. Med. Indones. 49 (2), 158–165.
Albalawi, A.E., Althobaiti, N.A., Alrdahe, S.S., Alhasani, R.H., Alaryani, F.S., BinMowyna, M.N., 2021. Anti-tumor effects of Queen Bee acid (10-Hydroxy-2-Decenoic Acid) alone and in combination with cyclophosphamide and its cellular mechanisms against ehrlich solid tumor in mice. Molecules 26 (22), 7021.
Arulselvan, P., Fard, M.T., Tan, W.S., Gothai, S., Fakurazi, S., Norhaizan, M.E., Kumar, S. S., 2016. Role of antioxidants and natural products in inflammation. Oxid. Med. Cell. Longev. 2016, 5276130.
Bao, F., Zhang, L., Pei, X., Lian, C., Liu, Y., Tan, H., Lei, P., 2021. MiR-20a-5p functions as a potent tumor suppressor by targeting PPP6C in acute myeloid leukemia. PLoS One 16 (9), e0256995.
Beishline, K., Azizkhan-Clifford, J., 2015. Sp1 and the 'hallmarks of cancer'. FEBS J. 282 (2), 224–258.
Carrillo-Sepulveda, M.A., Spitler, K., Pandey, D., Berkowitz, D.E., Matsumoto, T., 2015. Inhibition of TLR4 attenuates vascular dysfunction and oxidative stress in diabetic rats. J. Mol. Med. (Berl.) 93 (12), 1341–1354.
Chen, C.P., Lin, Y.C., Peng, Y.H., Chen, H.M., Lin, J.T., Kao, S.H., 2022a. Rosmarinic acid attenuates the lipopolysaccharide-provoked inflammatory response of vascular smooth muscle cell via inhibition of MAPK/NF-κb cascade. Pharmaceuticals (Basel) 15 (4), 437.
Chen, D.D., Wang, H.W., Cai, X.J., 2021. Transcription factor Sp1 ameliorates sepsis-induced myocardial injury via ZFAS1/notch signaling in H9C2 cells. Cytokine 140, 155426.
Chen, T., Ma, J., Liu, Y., Chen, Z., Xiao, N., Lu, Y., Fu, Y., Yang, C., Li, M., Wu, S., Wang, X., Li, D., He, F., Hermjakob, H., Zhu, Y., 2022b. iProX in 2021: connecting proteomics data sharing with big data. Nucleic Acids Res. 50(D1), D1522-D1527.
Collazo, N., Carpena, M., Nuñez-Estevez, B., Otero, P., Simal-Gandara, J., Prieto, MA., 2021. Health promoting properties of bee royal jelly: food of the queens. Nutrients 13 (2), 543.
Coutinho-Wolino, K.S., Almeida, P.P., Mafra, D., Stockler-Pinto, M.B., 2022. Bioactive compounds modulating toll-like 4 receptor (TLR4)-mediated inflammation: pathways involved and future perspectives. Nutr. Res. 107, 96–116.
Daenen, K., Andries, A., Mekahli, D., Van Schepdael, A., Jouret, F., Bammens, B., 2019. Oxidative stress in chronic kidney disease. Pediatr. Nephrol. 34 (6), 975–991.
Deguine, J., Barton, G.M., 2014. MyD88: a central player in innate immune signaling. F1000Prime Rep. 6, 97.
de Lima, R.S., Silva, J.C.S., Lima, C.T., de Souza, L.E., da Silva, M.B., Baladi, M.G., Irigoyen, M.C., Lacchini, S., 2019. Proinflammatory role of angiotensin II in the aorta of normotensive mice. Biomed Res. Int. 2019, 9326896.
Didion, S.P., Kinzenbaw, D.A., Schrader, L.I., Chu, Y., Faraci, F.M., 2009. Endogenous interleukin-10 inhibits angiotensin II-induced vascular dysfunction. Hypertension 54 (3), 619–624.
Dong, Y., Jin, C., Ding, Z., Zhu, Y., He, Q., Zhang, X., Ai, R., Yin, Y., He, Y., 2021. TLR4 regulates ROS and autophagy to control neutrophil extracellular traps formation against Streptococcus pneumoniae in acute otitis media. Pediatr. Res. 89 (4), 785–794.
Ejaz, M., Usman, S.M, Amir, S., Khan, M.J., 2023. Holistic expression of miR-17-92 cluster in obesity, kidney diseases, cardiovascular diseases, and diabetes. Mol. Biol. Rep. 50 (8), 6913–6925.
Eslami-Kaliji, F., Mirahmadi-Zare, S.Z., Nazem, S., Shafie, N., Ghaedi, R., Asadian-Esfahani, M.H., 2022. A label-free SPR biosensor for specific detection of TLR4 expression; introducing of 10-HDA as an antagonist. Int. J. Biol. Macromol. 217, 142–149.
Eslami-Kaliji, F., Sarafbidabad, M., Kiani-Esfahani, A., Mirahmadi-Zare, S.Z., Dormiani, K., 2021. 10-hydroxy-2-decenoic acid a bio-immunomodulator in tissue engineering; generates tolerogenic dendritic cells by blocking the toll-like receptor4. J. Biomed. Mater. Res. A. 109 (9), 1575–1587.
Fan, P., Han, B., Hu, H., Wei, Q., Zhang, X., Meng, L., Nie, J., Tang, X., Tian, X., Zhang, L., Wang, L., Li, J., 2020. Proteome of thymus and spleen reveals that 10-hydroxydec-2-enoic acid could enhance immunity in mice. Expert Opin. Ther. Targets 24 (3), 267–279.
Fan, P., Sha, F., Ma, C., Wei, Q., Zhou, Y., Shi, J., Fu, J., Zhang, L., Han, B., Li, J., 2022. 10-Hydroxydec-2-enoic acid reduces hydroxyl free radical-induced damage to vascular smooth muscle cells by rescuing protein and energy metabolism. Front. Nutr. 9, 873892.
Filali, M., Li, S., Kim, H.W., Wadzinski, B., Kamoun, M., 1999. Identification of a type 6 protein ser/thr phosphatase regulated by interleukin-2 stimulation. J. Cell Biochem. 73 (2), 153–163.
Gao, K., Su, B., Dai, J., Li, P., Wang, R., Yang, X., 2022. Anti-biofilm and Anti-hemolysis activities of 10-hydroxy-2-decenoic acid against *Staphylococcus aureus*. Molecules 27 (5), 1485.
Guo, J., Chen, X., Xi, R., Chang, Y., Zhang, X., Zhang, X., 2014. AEG-1 expression correlates with CD133 and PPP6c levels in human glioma tissues. J. Biomed. Res. 28 (5), 388–395.
Guven Maiorov, E., Keskin, O., Gursoy, A., Nussinov, R., 2013. The structural network of inflammation and cancer: merits and challenges. Semin. Cancer Biol. 23 (4), 243–251.
Han, L., Zhang, M., Li, F., Su, J., Wang, R., Li, G., Yang, X., 2023. 10-hydroxy-2-decenoic acid alleviates lipopolysaccharide-induced intestinal mucosal injury through anti-inflammatory, antioxidant, and gut microbiota modulation activities in chickens. Front. Microbiol. 14, 1285299.
He, A., Ji, R., Shao, J., He, C., Jin, M., Xu, Y., 2016. TLR4-MyD88-TRAF6-TAK1 Complex-mediated NF-κb activation contribute to the anti-inflammatory effect of V8 in LPS-induced Human cervical cancer SiHa cells. Inflammation 39 (1), 172–181.
Hernanz, R., Martínez-Revelles, S., Palacios, R., Martin, A., Cachofeiro, V., Aguado, A., García-Redondo, L., Barrús, M.T., de Batista, P.R., Briones, A.M., Salaices, M., Alonso, M.J., 2015. Toll-like receptor 4 contributes to vascular remodelling and endothelial dysfunction in angiotensin II-induced hypertension. Br. J. Pharmacol. 172 (12), 3159–3176.
Houdelet, C., Sinpoo, C., Chantaphanwattana, T., Voisin, S.N., Bocquet, M., Chantawannakul, P., Bulet, P., 2021. Proteomics of anatomical sections of the gut of

Nosema-infected western honeybee (*Apis mellifera*) reveals different early responses to *Nosema* spp. Isolates. J. Proteome Res. 20 (1), 804–817.
Huang, J., Liu, J., Chang, G., Wang, Y., Ma, N., Roy, A.C., Shen, X., 2021a. Glutamine supplementation attenuates the inflammation caused by LPS-induced acute lung injury in mice by regulating the TLR4/MAPK signaling pathway. Inflammation 44 (6), 2180–2192.
Huang, M., Dong, J., Tan, X., Yang, S., Xiao, M., Wang, D., 2023. Integration of metabolomic and transcriptomic provides insights into anti-inflammatory response to *trans*-10-hydroxy-2-decenoic acid on LPS-stimulated RAW 264.7 cells. Int. J. Mol. Sci. 24 (16), 12666.
Huang, M., Xiao, M., Dong, J., Huang, Y., Sun, H., Wang, D., 2022. Synergistic anti-inflammatory effects of graphene oxide quantum dots and trans-10-hydroxy-2-decenoic acid on LPS-stimulated RAW 264.7 macrophage cells. Biomater. Adv. 136, 212774.
Huang, S., You, S., Qian, J., Dai, C., Shen, S., Wang, J., Huang, W., Liang, G., Wu, G., 2021b. Myeloid differentiation 2 deficiency attenuates AngII-induced arterial vascular oxidative stress, inflammation, and remodeling. Aging (Albany NY) 13 (3), 4409–4427.
Interdonato, L., Impellizzeri, D., D'Amico, R., Cordaro, M., Siracusa, R., D'Agostino, M., Genovese, T., Gugliandolo, E., Crupi, R., Fusco, R., Cuzzocrea, S., Di Paola, R., 2023. Modulation of TLR4/nfκb pathways in autoimmune myocarditis. Antioxidants (Basel) 12 (8), 1507.
Ji, Y., Liu, J., Wang, Z., Liu, N., 2009. Angiotensin II induces inflammatory response partly via toll-like receptor 4-dependent signaling pathway in vascular smooth muscle cells. Cell Physiol. Biochem. 23 (4-6), 265–276.
Jiang, J.F., Zhou, Z.Y., Liu, Y.Z., Wu, L., Nie, B.B., Huang, L., Zhang, C., 2022. Role of Sp1 in atherosclerosis. Mol. Biol. Rep. 49 (10), 9893–9902.
Jiao, X., Yu, H., Du, Z., Li, L., Hu, C., Du, Y., Zhang, J., Zhang, X., Lv, Q., Li, F., Sun, Q., Wang, Y., Qin, Y., 2023. Vascular smooth muscle cells specific deletion of angiopoietin-like protein 8 prevents angiotensin II-promoted hypertension and cardiovascular hypertrophy. Cardiovasc. Res. 119 (9), 1856–1868.
Kawai, T., Akira, S., 2007. TLR signaling. Semin. Immunol. 19 (1), 24–32.
Kim, S.Y, Kang, H.T, Han, J.A, Park, S.C., 2012. The transcription factor Sp1 is responsible for aging-dependent altered nucleocytoplasmic trafficking. Aging Cell 11 (6), 1102–1109.
Kojima, H., Sasaki, T., Ishitani, T., Iemura, S.I., Zhao, H., Kaneko, S., Kunimoto, H., Natsume, T., Matsumoto, K., Nakajima, K., 2005. STAT3 regulates nemo-like kinase by mediating its interaction with IL-6-stimulated TGFβ-activated kinase 1 for STAT3 ser-727 phosphorylation. Proc. Natl. Acad. Sci. 102 (12), 4524–4529.
Kuo, G., Wu, C.Y., Yang, H.Y., 2019. MiR-17-92 cluster and immunity. J. Formos. Med. Assoc. 118 (1 Pt 1), 2–6.
Lamb, F.S., Choi, H., Miller, M.R., Stark, R.J., 2020. TNFα and reactive oxygen signaling in vascular smooth muscle cells in hypertension and atherosclerosis. Am. J. Hypertens. 33 (10), 902–913.
Lee, I.T., Lin, C.F., Huang, Y.L., Chong, K.Y., Hsieh, M.F., Huang, T.H., Cheng, C.Y., 2019. Protective mechanisms of resveratrol derivatives against TNF-α-induced inflammatory responses in rat mesangial cells. Cytokine 113, 380–392.
Leung, A., Stapleton, K., Natarajan, R., 2016. Functional long non-coding RNAs in vascular smooth muscle cells. Curr. Top. Microbiol. Immunol. 394, 127–141.
Lewis, B.P., Burge, C.B., Bartel, D.P., 2005. Conserved seed pairing, often flanked by adenosines, indicates that thousands of human genes are microRNA targets. Cell 120 (1), 15–20.
Li, J., Jia, Z., Zhang, Q., Dai, J., Kong, J., Fan, Z., Li, G., 2021. Inhibition of ERK1/2 phosphorylation attenuates spinal cord injury induced astrocyte activation and inflammation through negatively regulating aquaporin-4 in rats. Brain Res. Bull. 170, 162–173.
Li, R., Xiao, J., Qing, X., Xing, J., Xia, Y., Qi, J., Liu, X., Zhang, S., Sheng, X., Zhang, X., Ji, X., 2015. Sp1 mediates a therapeutic role of MiR-7a/b in angiotensin II-induced cardiac fibrosis via mechanism involving the TGF-β and MAPKs pathways in cardiac fibroblasts. PLoS One 10 (4), e0125513.
Lin, X.M., Liu, S.B., Luo, Y.H., Xu, W.T., Zhang, Y., Zhang, T., Xue, H., Zuo, W.B., Li, Y.N., Lu, B.X., Jin, C.H., 2020. 10-HDA induces ROS-mediated apoptosis in A549 human lung cancer cells by regulating the MAPK, STAT3, NF-κB, and TGF-β1 signaling pathways. Biomed. Res. Int. 2020, 3042636.
Liu, G., Lu, Y., Shi, L., Ren, Y., Kong, J., Zhang, M., Chen, M., Liu, W., 2020. TLR4-MyD88 signaling pathway is responsible for acute lung inflammation induced by reclaimed water. J. Hazard. Mater. 396, 122586.
Liu, J., Li, G., Xie, W.J., Wang, L., Zhang, R., Huang, K.S., Zhou, Q.S., Chen, D.C., 2017. Lipopolysaccharide stimulates surfactant protein-A in human renal epithelial HK-2 cells through upregulating toll-like receptor 4 dependent MEK1/2-ERK1/2-NF-κB pathway. Chin. Med. J. 130 (10), 1236–1243.
Lu, Y.C., Yeh, W.C., Ohashi, P.S., 2008. LPS/TLR4 signal transduction pathway. Cytokine 42 (2), 145–151.
Ma, C., Ahmat, B., Li, J., 2022. Effect of queen cell numbers on royal jelly production and quality. Curr. Res. Food Sci. 5, 1818–1825.
Ma, J., Chen, T., Wu, S., Yang, C., Bai, M., Shu, K., Li, K., Zhang, G., Jin, Z., He, F., Hermjakob, H., Zhu, Y., 2019. iProX: an integrated proteome resource. Nucleic Acids Res. 47(D1), D1211-D1217.
MacDowell, K.S, Pinacho, R., Leza, J.C., Costa, J., Ramos, B., García-Bueno, B., 2017. Differential regulation of the TLR4 signalling pathway in post-mortem prefrontal cortex and cerebellum in chronic schizophrenia: relationship with SP transcription factors. Prog. Neuropsychopharmacol. Biol. Psychiatry 79 (Pt B), 481–492.
Mariani, V., Biasini, M., Barbato, A., Schwede, T., 2013. lDDT: a local superposition-free score for comparing protein structures and models using distance difference tests. Bioinformatics 29 (21), 2722–2728.
Mehra, V.C., Ramgolam, V.S., Bender, J.R., 2005. Cytokines and cardiovascular disease. J. Leukoc. Biol. 78 (4), 805–818.
Meng, Z., Si, C.Y., Teng, S., Yu, X.H., Li, H.Y., 2019. Tanshinone IIA inhibits lipopolysaccharide-induced inflammatory responses through the TLR4/TAK1/NFκB signaling pathway in vascular smooth muscle cells. Int. J. Mol. Med. 43 (4), 1847–1858.
Mita, Y., Dobashi, K., Endou, K., Kawata, T., Shimizu, Y., Nakazawa, T., Mori, M., 2002. Toll-like receptor 4 surface expression on human monocytes and B cells is modulated by IL-2 and IL-4. Immunol. Lett. 81 (1), 71–75.
Nabata, T., Fukuo, K., Morimoto, S., Kitano, S., Momose, N., Hirotani, A., Nakahashi, T., Nishibe, A., Hata, S., Niinobu, T., Suhara, T., Shimizu, M., Ohkuma, H., Sakurai, S., Nishimaki, H., Ogihara, T., 1997. Interleukin-2 modulates the responsiveness to angiotensin II in cultured vascular smooth muscle cells. Atherosclerosis 133 (1), 23–30.
Ohto, U., Fukase, K., Miyake, K., Shimizu, T., 2012. Structural basis of species-specific endotoxin sensing by innate immune receptor TLR4/MD-2. Proc. Natl. Acad. Sci. 109 (19), 7421–7426.
Park, H.J., Kim, B., Koo, D.B., Lee, D.S., 2021. Peroxiredoxin 1 controls ovulation and ovulated cumulus-oocyte complex activity through TLR4-derived ERK1/2 signaling in mice. Int. J. Mol. Sci. 22 (17), 9437.
Qu, R.N., Qu, W., 2019. Metformin inhibits LPS-induced inflammatory response in VSMCs by regulating TLR4 and PPAR-γ. Eur. Rev. Med. Pharmacol. Sci. 23 (11), 4988–4995.
Rocha, D.M., Caldas, A.P., Oliveira, L.L., Bressan, J., Hermsdorff, H.H., 2016. Saturated fatty acids trigger TLR4-mediated inflammatory response. Atherosclerosis 244, 211–215.
Saraiva, M., O'Garra, A., 2010. The regulation of IL-10 production by immune cells. Nat. Rev. Immunol. 10 (3), 170–181.
Satoh, K., Nigro, P., Berk, B.C., 2010. Oxidative stress and vascular smooth muscle cell growth: a mechanistic linkage by cyclophilin A. Antioxid. Redox. Signal. 12 (5), 675–682.
Sha, F., Yang, P., Wang, H., Ren, J., Li, Z., Zhang, L., Fan, P., 2023. 10-Hydroxydec-2-enoic acid enhances the erythrocyte membrane fluidity via interacting with phosphatidylcholine and phosphatidylethanolamine. Ital. J. Food Sci. 35 (4), 119–129.
Shi, C., Tan, J., Lu, J., Huang, J., Li, X., Xu, J., Wang, X., 2022. MicroRNA-17-5p promotes vascular calcification by targeting ANKH. Curr. Neurovasc. Res. 19 (1), 108–116.
Sousa-Lopes, A., de Freitas, R.A., Carneiro, F.S., Nunes, K.P., Allahdadi, K.J., Webb, R.C., de Cassia Tostes, R., Giachini, F.R., Lima, V.V., 2020. Angiotensin (1-7) inhibits Ang II-mediated ERK1/2 activation by stimulating MKP-1 activation in vascular smooth muscle cells. Int. J. Mol. Cell. Med. 9 (1), 50–61.
Sprague, A.H., Khalil, R.A., 2009. Inflammatory cytokines in vascular dysfunction and vascular disease. Biochem. Pharmacol. 78 (6), 539–552.
Sun, J., Ding, Y., 2012. NOD2 agonist promotes the production of inflammatory cytokines in VSMC in synergy with TLR2 and TLR4 agonists. Sci.WorldJ. 2012, 607157.
Suo, L., Wang, M., 2022. Dexmedetomidine attenuates oxygen-glucose deprivation/reperfusion-induced inflammation through the miR-17-5p/ TLR4/ NF-κB axis. BMC Anesthesiol. 22 (1), 126.
Uchida, H.A., Takatsuka, T., Hada, Y., Umebayashi, R., Takeuchi, H., Shikata, K., Subramanian, V., Daugherty, A., Wada, J., 2022. Edaravone attenuated angiotensin II-induced atherosclerosis and abdominal aortic aneurysms in apolipoprotein E-deficient mice. Biomolecules 12 (8), 1117.
Vizcaíno, C., Mansilla, S., Portugal, J., 2015. Sp1 transcription factor: a long-standing target in cancer chemotherapy. Pharmacol. Ther. 152, 111–124.
Wang, D., Westerheide, S.D., Hanson, J.L., Baldwin Jr., A.S., 2000. Tumor necrosis factor alpha-induced phosphorylation of RelA/p65 on Ser529 is controlled by casein kinase II. J. Biol. Chem. 275 (42), 32592–32597.
Wang, H., Huang, M., Wang, W., Zhang, Y., Ma, X., Luo, L., Xu, X., Xu, L., Shi, H., Xu, Y., Wang, Ai., Xu, T., 2021. Microglial TLR4-induced TAK1 phosphorylation and NLRP3 activation mediates neuroinflammation and contributes to chronic morphine-induced antinociceptive tolerance. Pharmacol. Res. 165, 105482.
Wang, J., Xie, S.A., Li, N., Zhang, T., Yao, W., Zhao, H., Pang, W., Han, L., Liu, J., Zhou, J., 2022. Matrix stiffness exacerbates the proinflammatory responses of vascular smooth muscle cell through the DDR1-DNMT1 mechanotransduction axis. Bioact. Mater. 17, 406–424.
Wasiluk, K.R., McCulloch, K.A., Banton, K.L., Dunn, D.L., 2006. Sp1 elements regulate transcriptional activity within the murine Toll-like receptor 4 promoter. Surg. Infect. (Larchmt) 7 (6), 489–499.
Yang, W., Tian, Y., Han, M., Miao, X., 2017. Longevity extension of worker honey bees (*Apis mellifera*) by royal jelly: optimal dose and active ingredient. PeerJ 5, e3118.
Yang, Y.C., Chou, W.M., Widowati, D.A., Lin, I.P., Peng, C.C., 2018. 10-hydroxy-2-decenoic acid of royal jelly exhibits bactericide and anti-inflammatory activity in human colon cancer cells. BMC Complement. Altern. Med. 18 (1), 202.
Ye, Y., Bian, W., Fu, F., Hu, J., Liu, H., 2018. Selenoprotein S inhibits inflammation-induced vascular smooth muscle cell calcification. J. Biol. Inorg. Chem. 23 (5), 739–751.
You, M., Miao, Z., Pan, Y., Hu, F., 2019. Trans-10-hydroxy-2-decenoic acid alleviates LPS-induced blood-brain barrier dysfunction by activating the AMPK/PI3K/AKT pathway. Eur. J. Pharmacol. 865, 172736.
Yu, T., Wang, T., Kuang, S., Zhao, G., Zhou, K., Zhang, H., 2021. A microRNA-17-5p/homeobox B13 axis participates in the phenotypic modulation of vascular smooth muscle cells. Mol. Med. Rep. 24 (4), 731.

Yu, T.K., Caudell, E.G., Smid, C., Grimm, E.A., 2000. IL-2 activation of NK cells: involvement of MKK1/2/ERK but not p38 kinase pathway. J. Immunol. 164 (12), 6244–6251.
Zhang, C., Wang, N., Tan, H.Y., Guo, W., Chen, F., Zhong, Z., Man, K., Tsao, S.W., Lao, L., Feng, Y., 2020. Direct inhibition of the TLR4/MyD88 pathway by geniposide suppresses HIF-1α-independent VEGF expression and angiogenesis in hepatocellular carcinoma. Br. J. Pharmacol. 177 (14), 3240–3257.
Zhang, L., Yang, P., Chen, J., Chen, Z., Liu, Z., Feng, G., Sha, F., Li, Z., Xu, Z., Huang, Y., Shi, X., Li, X., Cui, J., Zhang, C., Fan, P., Cui, L., Shen, Y., Zhou, G., Jing, H., Ma, S., 2023. CD44 connects autophagy decline and ageing in the vascular endothelium. Nat. Commun. 14 (1), 5524.
Zhao, W., Gupta, A., Krawczyk, J., Gupta, S., 2022. The miR-17-92 cluster: Yin and Yang in human cancers. Cancer Treat. Res. Commun. 33, 100647.
Zheng, J., Lai, W., Zhu, G., Wan, M., Chen, J., Tai, Y., Lu, C., 2013. 10-Hydroxy-2-decenoic acid prevents ultraviolet A-induced damage and matrix metalloproteinases expression in human dermal fibroblasts. J. Eur. Acad. Dermatol. Venereol. 27 (10), 1269–1277.
Zheng, J., Zhang, R., Liu, C., Yang, H., Jin, X., 2023. The TLR4/NF-κB signaling pathway-mediated type 2 skewing of T helper cell in cough variant asthma was counteracted by ethanol extract of Anacyclus pyrethrum root. Immunobiology 228 (3), 152379.
Zhou, G., Soufan, O., Ewald, J., Hancock, R.E.W., Basu, N., Xia, J., 2019. NetworkAnalyst 3.0: a visual analytics platform for comprehensive gene expression profiling and meta-analysis. Nucleic Acids Res. 47 (W1), W234–W241.
Zhou, X., Yuan, P., He, Y., 2012. Role of microRNAs in peripheral artery disease (review). Mol. Med. Rep. 6 (4), 695–700.
Zhu, Y., Jiang, X., Zhang, S., Wang, L., Zhou, Q., Jiang, J., 2020. Hsa_circ_103973 acts as a sponge of miR-335 to promote cervical cancer progression. Onco. Targets Ther. 13, 1777–1786.
Zhu, Y., Qu, J., He, L., Zhang, F., Zhou, Z., Yang, S., Zhou, Y., 2019. Calcium in vascular smooth muscle cell elasticity and adhesion: novel insights into the mechanism of action. Front. Physiol. 10, 852.